In presenting the dissertation as a partial fulfillment of the requirements for an advanced degree from the Georgia Institute of Technology, I agree that the Library of the Institute shall make it available for inspection and circulation in accordance with its regulations governing materials of this type. I agree that permission to copy from, or to publish from, this dissertation may be granted by the professor under whose direction it was written, or, in his absence, by the Dean of the Graduate Division when such copying or publication is solely for scholarly purposes and does not involve potential financial gain. It is understood that any copying from, or publication of, this dissertation which involves potential financial gain will not be allowed without written permission.

7/25/68

DISLOCATION INTERACTIONS AT INTERFACES

A THESIS

Presented to

The Faculty of the Division of Graduate

Studies and Research

by

Billy Ray Livesay

In Partial Fulfillment

of the Requirements for the Degree

Doctor of Philosophy in the School

of Chemical Engineering

Georgia Institute of Technology

March, 1972

DISLOCATION INTERACTIONS AT INTERFACES

Approved:

Chairman

Date approved by Chairman: Feb. 23 1972

ACKNOWLEDGMENTS

The author wishes to express his strong appreciation to his advisor, Dr. E. A. Starke, Jr., for his personal enthusiasm, inspiration, and patient guidance in the course of this work. The author is greatly indebted to Dr. E. J. Scheibner for his sustaining personal and professional encouragement, without which this work would never have been attempted. He also wishes to thank Dr. N. N. Engel for his helpful suggestions as a member of the reading committee.

Support by A.F.O.S.R. under project THEMIS contract F44620-68-C-008 and under grant AFOSR-71-2064 and support by ONR/ARPA under contract Nonr-991(15) is deeply appreciated.

Special thanks are due to Mrs. Mary Floyd and Mrs. Caron Crane for their patience in typing the final manuscript.

The greatest gratitude of the author is reserved for his wife, Ann, and children, Connie, Cathy and Douglas, for their continued faith and love which made the work possible.

TABLE OF CONTENTS

TABLE OF CONTENTS (Continued)

LIST OF TABLES

LIST OF FIGURES

Figure Page

SUMMARY

The mechanical behavior of structural materials is influenced by material parameter discontinuities which occur at interfaces. The principal interface factors affecting dislocation dynamics near an abrupt interface are differences in elastic moduli, lattice parameter misfit, crystallographic structure and orientation and interfacial impurities. The development of models for predicting the behavior of a particular material configuration requires a detailed understanding of how the various interfacial parameters influence mechanical deformation processes. The objective of the work reported here was to investigate the effect on mechanical behavior of a differential modulus across an interface of single crystal composite samples prepared in configurations which minimized the influence of other factors.

Tensile specimens were prepared from thin copper single crystals and epitaxial metal films were grown on the surfaces by vapor deposition to provide desired interfaces. The principal material combinations studied were copper-nickel and copper-cobalt. In addition, copper films grown onto copper tensile specimen substrates were used to evaluate the influence of certain imperfections.

The elastic modulus difference was found to provide the primary strengthening mechanism for Cu-Ni and Cu-Co interfaces. An abrupt interface, small lattice misfit and compatible crystal structures are required for this factor to play a dominant role. Surface and interfacial energy terms were also evaluated and found not significant

compared to contributions from other interface factors. Crystal structure changes induced in cobalt coatings with deformation resulted in high work-hardening compared to that of the Cu-Ni systems.

CHAPTER I

INTRODUCTION

The effect of an interface on the mechanical behavior of a metal involves a number of complex phenomena whose fundamental contributions are not easily determined. Even a relatively simple interface such as that occurring at the surface of a metal in a vacuum involves discontinuities in all the bulk properties of the material. To predict the behavior of even such a simple system requires a knowledge of how the surface alters the various physical and chemical parameters of the material and in turn, how these parameters influence mechanical behavior. When a second material is allowed to react with the base metal, consideration must then be given to additional factors such as atomic bonding mechanisms between the base metal and the coating, the coating configuration and the various physical and chemical properties of the coating. The latter are probably significantly different from what they would be in bulk form.

A usable scheme for predicting the behavior of a particular material configuration would require an understanding of how the various interfacial parameters influence mechanical deformation processes. In practical situations it will probably be necessary to construct a loop analysis involving the effect of interface parameters on mechanical deformation with the deformation itself altering interfacial parameters and thereby influencing subsequent deformation.

The mechanical behavior of crystalline solids is primarily explainable in terms of the dynamics of dislocations. The elastic stress field resulting from the presence of a dislocation is long ranged and accounts for the interactions of dislocations with other dislocations and with such features as grain boundaries, precipitates, impurity atoms, surfaces and a variety of interfaces. Treatments of dislocation mechanics are covered in comprehensive texts.[1,2,3] Material discontinuities such as free surfaces or interfaces modify the stress field and there is a tendency for dislocation motion to lower the strain energy, e.g., a dislocation near a free surface will tend to move towards the surface in order to relieve the strain within the crystal.

The principal factors influencing dislocation dynamics in the neighborhood of an abrupt interface are outlined below:

(a) Elastic modulus. The relative shear modulus on either side of an interface influences the strain field of a dislocation and therefore its dynamical behavior in the sample[4-13] although the magnitude of the effect is uncertain.[14-25]

(b) Lattice parameter. A lattice parameter misfit across an interface coupled with the interfacial energy influences the degree of coherency[26-32] and slip through the interface since the magnitude of the Burgers vector must always be conserved.

(c) Crystal structure and orientation. Crystal structure and/or orientation changes across an interface may impede dislocation motion by altering either the Peierls force or the resolved stress.

(d) Impurities. Impurities at an interface may present pinning points either for dislocation sources or for hardening processes.

(e) Continuity and environment. The magnitude of the influence of interface parameters will be related to the integrity of the coating. Changes occurring during deformation or due to the environment[33-46] may significantly alter mechanical behavior.

The objective of the work reported herein was to investigate the effect on mechanical behavior of a differential modulus across an interface of single crystal composite samples prepared in configurations which minimized the influence of other factors.

CHAPTER II

BACKGROUND

The effect of surface and environmental conditions on the performance of materials in service has been well documented. Geometrical configurations, e.g., notches and scratches, act as stress risers and are known to have a detrimental effect on mechanical properties. In addition, the state of stress of the surface in combination with various environmental conditions can affect such properties as fatigue life and stress corrosion susceptibility, two of the primary causes of service failures. The manner in which geometrical and environmental parameters influence performance varies greatly from material to material, and, since environmental reactions are primarily with the surface, their effect may be determined by the surface phase.

One of the earliest demonstrations of the significance of surface coatings on the mechanical behavior of metals is found in the simple experiments of Roscoe.[14] He found the resolved shear stress of small cadmium single crystal wires to be significantly increased after thermally growing a thick oxide film on the surface. Their previous strength was obtained by removing the oxide with dilute sulphuric acid. The calculated increased strength of the oxide coated wires was far in excess of what one would expect from the direct load carrying capacity of the oxide film. Even with the oxide severely fractured, the yield point was still higher than for the uncoated wires. Since Roscoe's

early work, a number of experiments and several theoretical treatments have demonstrated the importance of surface coatings on the mechanical properties of metals and alloys.

Quantitative theoretical treatments of the problem of dislocations near material discontinuities are difficult and only a few simple configurations have been considered in any detail. A direct calculation of the energy content of such stress fields involves a boundary value problem at the interface. Eshelby[4] greatly simplified the problem with the assumption of a series of image dislocations which produce fictitious stress fields that satisfy the boundary conditions required at the interface. This type of treatment is analogous with that used in electrostatic potential field calculations. Force calculations are then carried out by assuming the imaginary dislocations are real and vectorially summing to obtain the net force on the real dislocation due to the one or more imaginary dislocations. The imaginary dislocations are called "image dislocations" just as the imaginary charges in electrostatics are called "image charges." Use has been made of Eshelby's concept of image dislocations to solve boundary value problems for several important idealized dislocation-interface configurations. Although it is difficult to directly apply the available theoretical results to real conditions, they do provide insight for the interpretation of certain experimental observations.

Head[5,6] considered several configurations involving screw dislocations near an interface. For a single screw dislocation in a medium of elastic modulus, μ_1, near a coherent interface with a medium of elastic modulus, μ_2, he found that for $\mu_2 < \mu_1$ the dislocation is

attracted to the interface and for $\mu_1 < \mu_2$ the dislocation is repelled. The magnitude of the forces involved in each case is determined by assigning a value of $\frac{\mu_2 - \mu_1}{\mu_2 + \mu_1} \vec{b}$ for the Burgers vector of the image dislocations located at x = -a with the real dislocation having Burgers vector $\vec{b}$ at x = +a.

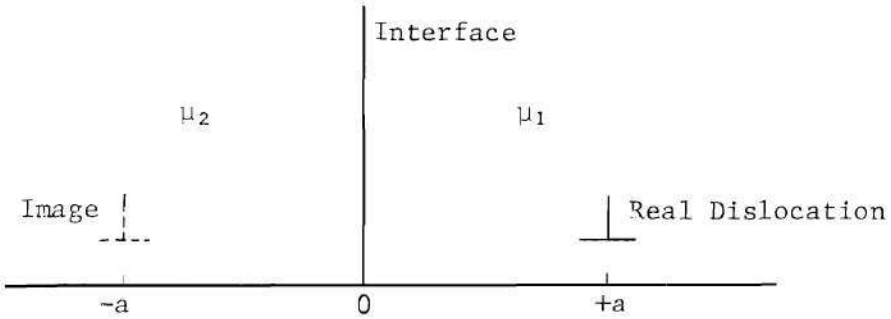

Figure 1. Dislocation and Image Near Interface of Two Semi-Infinite Solids

The force acting on the real dislocation due to the presence of the interface is then given by

$$F_x = \left(\frac{\mu_2 - \mu_1}{\mu_2 + \mu_1}\right) \mu_1 \frac{b^2}{4\pi a} \quad .$$

However, since the dislocation core involves material strained beyond the elastic region, the above expression for F_x breaks down for $a \leq 2b$. For the case of a free surface, $\mu_2 = 0$, the dislocation is always attracted towards the surface with a magnitude proportional to the inverse first power of the distance from the surface.

An infinite series of image dislocations is required to satisfy the boundary conditions for a screw dislocation within a substrate of

modulus μ_1 coated with a film of thickness t and modulus μ_2. For $\mu_2 < \mu_1$ the dislocation is always attracted to the surface but for $\mu_2 > \mu_1$, there exists an equilibrium position, or energy well, at some distance from the interface depending upon the values of μ_1, μ_2 and t. Head[6] extended his calculation to a model involving a pile up of n dislocations where the barrier is a film of thickness t and estimates the number of dislocations the barrier can support.

Head's models involve screw dislocations oriented parallel to the plane of the interface. Eshelby and Stroh[7] applied the image concept to straight screw dislocations in a thin plate with free surfaces but oriented perpendicular to the plane of the plate. They found the force between two such dislocations to be short-ranged, behaving as $r^{-1} \exp(-\alpha r)$. Yoffe[8] has derived expressions for the stress field of a general dislocation intersecting a free surface at any angle in a semi-infinite isotropic solid.

Conners[9] carried out similar stress field calculations for a straight edge dislocation. The glide force, F_G, acting on a pure edge dislocation a distance, a, from a free surface is, according to Conners

$$F_G = \frac{bb_2\mu}{4\pi(1 - \nu)a} \quad .$$

The direction of the glide force on the dislocation is towards the surface along the glide direction and b_2 is the component of the Burgers vector, $\vec{b}$, normal to the surface. Both Conners and Head showed an inverse dependence on distance from the surface for the interaction force. Conners also considered the case where the surface has a bonded

coating of thickness t. The substrate and coating are assumed to have the same Poisson's ratio and respective Young's moduli, E_s and E_c. For the simplified case where the slip plane is normal to the interface, the interaction force takes the form[9]

$$F = \frac{\mu b^2}{4\pi(a + t)(1 - \nu)} \left[1 - \left(\frac{E_c}{E_s + E_c}\right)^2 \left(K_1 + \frac{t}{t + a} K_2\right)\right]$$

where

$$K_1 = (1 - \nu)\left(\frac{1}{1 - 2\nu} + \frac{1}{2 - \nu}\right)$$

$$K_2 = \left(\frac{1 - \nu}{4}\right)\left(\frac{2 + 4\nu}{1 - 2\nu} - \frac{1}{2 - \nu}\right) .$$

Letting $\nu = 1/4$, $\beta \equiv E_c/(E_s + E_c)$ and assuming a coating thickness of 5b, very low values of β result in the interface always attracting, and sufficiently high values of β always repelling, the dislocation. For a narrow range of relative moduli, positions are determined where the net force on a dislocation is zero.

McNeil and Grosskreutz[10] applied the analysis of Conners to the case of dislocation dipoles near an interface. A dislocation dipole consists of two dislocations of the same kind having Burgers vectors of equal magnitude but opposite sign and located a small distance apart. As with electrostatic and magnetic dipoles, the interaction field is very short ranged, going as r^{-3}. Surface and coating dipole image interaction forces were found to be negligible within the approximations of their calculations.

Prins and Wilsdorf[11] evaluated the effect of a surface on the interaction forces between two dislocations on neighboring parallel slip planes. Their calculations were for screw-screw and edge-edge interactions on slip planes having various separations and making various angles with the surface normal. For example, it was shown that two screw dislocations of the same sign will always be able to pass one another near the surface if they could have passed in the bulk. However, opposite signs require greater passing stresses near the surface than in the bulk and may act as an effective barrier for dislocation egress provided the angle between the slip plane and the surface normal is not greater than about 75 degrees. Edge dislocations have a more complex interaction. These calculations treat only dislocations on parallel slip planes at a material-vacuum interface and are therefore very specific.

Koehler[12] has recently described several interface systems which might be prepared as a multiple layered composite structure. Considering only the effect of a differential elastic modulus across an interface he showed that significant strengthening should occur in composite pairs having epitaxial interfaces such as nickel-copper, rhodium-palladium, platinum-iridium, MgO-LiF and tungsten-tantalum. For the differential modulus effect to be significant it is important that the interfaces between the two components be abrupt. Fleischer[13] estimated the effect of a gradual change in both the elastic modulus and lattice parameter relative to an abrupt change and found the effect produced by a gradual change to be negligible compared to other factors.

Early demonstrations of the inhibiting effect of surface coatings on dislocation egress include the experiments of Roscoe[14] and Barrett[15] using metal-metal oxide interfaces and Gilman and Read[16] using selected metal-metal interfaces. Brame and Evans[17] grew oriented single crystal films of several different metals on silver single crystal substrates. Subsequent to straining the composite samples about 15%, examination of the coatings stripped from the substrates showed that dislocations are injected into the coating from sources activated within the substrate. Depending upon the film structure, films either slipped along slip lines in the substrate, cracked along substrate lines or cracked normal to the stress axis but with no relationship to substrate slip lines. They concluded that the degree of misfit had the greatest influence on the passage of dislocations from the substrate into the film and proposed two processes which could impede dislocations. First an accommodating network of dislocations[26] occurs at the interface to lower the elastic strain energy associated with the misfit. Secondly, a change in lattice spacing on the active slip plane would result in a displacement residue[2] at the interface due to the required change in Burgers vector as the dislocation cuts the interface. The passage of additional dislocations would increase the displacement residue in some manner. Subsequent experiments[18] demonstrated that the degree to which a surface film influences slip processes in the substrate depends upon the adherence of the film to the substrate.

The stress field of a residue, $\Delta\vec{b}$, should have a functional behavior similar to that of normal dislocations.[2] For a dislocation transmitted on a common slip plane from one medium where the Burgers

vector is $\vec{b}_1$ into a second medium where the Burgers vector is $\vec{b}_2$, $\Delta\vec{b} = \vec{b}_1 - \vec{b}_2$. For $b_1 > b_2$, the residue will have the same sign as both $\vec{b}_1$ and $\vec{b}_2$ and therefore repel coplanar dislocations with Burgers vectors $\vec{b}_1$ in the first medium and $\vec{b}_2$ in the second. For $b_2 > b_1$, the corresponding interaction forces would be attractive. The actual configuration assumed by the accumulation of n residues due to the transmission of n dislocations apparently has never been confirmed. Fleischer[13] pictures the accumulation occurring with increments of $\vec{b}_1 - \vec{b}_2$ piling up on successive atomic displacements. An alternative concept accumulates the net residue at the interface or within a few atomic distances. The difference is not important for the passage of less than $b_2/(b_1 - b_2)$ dislocations on an active glide plane. If the accumulation is essentially localized it is reasonable to assume that as n becomes large enough for $n(\vec{b}_1 - \vec{b}_2) \approx \vec{b}_2$ then the net residue can propagate into the coating lattice. The localized accumulation model would therefore result in a periodic coherency stress field on an active slip system whereas the stress from the pile-up model would increase monotonically. The validity of the residue pile-up model is questionable since the driving force for the generation of residues drops sharply as the distance from the interface increases.

Accommodating dislocations have been shown to be generated as the coating thickness increases[29-31] during growth of a coating. The accommodating dislocations are thought to be an accumulation of normal glide dislocations which move into the interface region to decrease the net lattice strain energy. The stress field of such a network is short ranged,[2] decreasing exponentially with displacement from the

interface and is effective for a distance approximately equal to that of the grid spacing. The magnitude of the frictional force on dislocations by a rigid accommodation grid is determined by a number of geometrical factors associated with the relative orientation of dislocation segments and Burgers vectors and with grid spacing. A dislocation line oriented so that it cuts the network with only the creation of jogs experiences little resistance. However, where segments of a glide dislocation are attracted by elements of the grid, relatively strong interaction forces may result.

Latanision and Staehle[20] found a marked strengthening effect produced by the growth of an oxide film on nickel single crystals using stressed electrode experiments. A crystal strained during dissolution was found to have larger slip steps which were farther apart than those occurring on the surface of a sample strained in air.

Recently reported measurements of Ruddle and Wilsdorf[21] showed a significantly lower yield stress for copper single crystals electroplated with nickel as compared to unplated crystals. These results directly contradict the behavior expected considering only the relative elastic moduli of the two materials. They proposed that the accommodating dislocation network leads to easy nucleation of additional glide dislocations when stress is applied. Very recent results reported by Patterson and Greenfield[24] using copper-nickel and copper-gold systems and even later by Pridans and Bilello[25] for the copper-chromium system showed only strengthening produced by the coating. Johnson and Block[22] investigated the mechanical effects of widely varied electroplated coatings and also reported only strengthening. Patterson and Greenfield

found strengthening occurred in both the Cu-Ni system where the modulus difference is large and lattice misfit is small and in the Cu-Au system where the lattice misfit is large and the modulus difference is negative. They also introduced an additional interface factor, solid solution hardening, by surface alloying a number of their samples and found that significant strengthening occurred. The coatings of Patterson and Greenfield were vapor deposited in high vacuum as compared with the electroplating technique employed by Ruddle and Wilsdorf and therefore the method of film deposition may account for the difference in their results. The coatings of Pridans and Bilello were also electroplated but chromium has a body centered cubic crystal structure and a relatively high temperature was used for their plating bath. Each of these investigating teams reported evidence of epitaxy in their films. Johnson and Block[22] proposed that substrate surface damage is the primary strengthening mechanism for the various coatings they plated onto copper crystals. However, Pridans and Bilello[25] found no strengthening effect for a copper crystal stressed, electroplated with chromium and subsequently stripped and restressed. Pridans and Bilello[25] proposed that the major interface strengthening is due to the activation of secondary slip systems by back stresses resulting from direct interface interactions.

A wide range of evidence demonstrates the importance of surface and interface parameters on mechanical behavior. A number of theoretical models have been proposed suggesting mechanisms which could account for observed behavior, whether the net effect is one of increased or decreased strength. However, theoretical developments have not been

sufficiently specific to allow direct comparisons between theory and experiment. The number of interface systems investigated experimentally is small and problems with actually achieving a desired interface configuration are not trivial.

CHAPTER III

EXPERIMENTAL APPROACH AND PROCEDURES

Experimental Approach

An ideal interface system for experimental investigations of mechanical effects of a differential elastic modulus would be planar, abrupt, and coherent interface between two crystals where the two components have mechanical, chemical and crystallographic characteristics identical except for the elastic modulus. However, this situation cannot be realized in practice so experimental investigations of a particular interface factor are best carried out using simple material configurations which either minimize or hold constant the influence of other factors. In the study reported here tensile specimens were prepared from thin copper single crystals. Epitaxial metal films were grown on the surfaces to provide desired interfaces. Effects of the resulting interfaces were then investigated using mechanical measurements and subsequent microscopic examinations.

The two principal material combinations selected for study were copper-nickel and copper-cobalt. Although larger modulus differences are possible using other material combinations, chemical and crystallographic considerations make Cu-Ni and Cu-Co particularly useful. The structures of copper and nickel are face-centered cubic and reliable vacuum preparation procedures allow epitaxial coatings of nickel to be deposited on copper crystals. The lattice misfit between copper and

nickel is only 2.5% and the elastic modulus difference is 54%. The copper-cobalt system introduces a possible additional factor in that the room temperature equilibrium structure of bulk cobalt is hexagonal close-packed. However, sufficiently thin cobalt films grown on copper crystals can be prepared with an fcc structure. Thick films develop hcp regions which may be considered as faulted fcc. The modulus difference for the copper-cobalt interface is 69% with a lattice misfit of 2.0% for fcc cobalt. Copper films grown onto copper tensile specimen substrates were used to evaluate the effect of interface imperfections associated with the preparation techniques.

Single crystals were used for the tensile specimen substrates to eliminate grain boundary contributions. Substrate thicknesses between 30-100 microns were employed so that the bulk strength of the substrate would not mask interface effects. However, this thickness should be sufficiently large for initial dislocation processes within the crystal bulk to not be strongly influenced by surface effects.

Measurement uncertainties associated with variations in the bulk behavior of the substrate material were minimized by making quantitative comparisons only between specimens of a single set. A set consisted of the several specimens machined co-directionally from one thin single crystal wafer. This insured identical crystallographic orientation, and considerable care was taken to see that all substrates of a particular set had identical thermo-mechanical histories. For each set, metal-metal interfaces were prepared using two substrates and one specimen was left with free surfaces. All measurements were made at room temperature

in air. The stress rate was determined by applied loading rates near 6.6×10^3 dyne/sec.

Procedures

Sample Preparation

A detailed description of the sample preparation technique is provided in Appendix A. Large single crystals of copper were radiation hardened using a cumulative dosage of about 10^{18} neutrons/cm^2. Wafers were spark sliced along particular planes from the hardened crystals and subsequently spark planed, mechanically polished and then electropolished to a uniform thickness in the desired range. Four or five tensile specimen substrates with a gauge length and width of 7 mm and 2 mm respectively were photomachined from each wafer. Radiation hardening was then removed by vacuum annealing. The stress axis was defined by proper orientation of the photo mask which cast multiple identical and parallel sample images. Back reflection Laue patterns of the machined tensile specimens were used to determine the resulting crystalographic orientation to an accuracy of about one degree. The crystallographic orientation of tensile specimen sets employed in this study are shown Figure 2.

The validity of making quantitative comparisons between specimens belonging to a single set was verified with pairs of tensile samples machined co-directionally from wafers of several orientations. The force-displacement curves for pairs agreed within a few percent. The gauge sections of these specimens were 3.0 mm wide instead of the 2.0 mm width later adopted for the specimens used in the interface investigations and therefore slip lines were observed extending into the 4.0

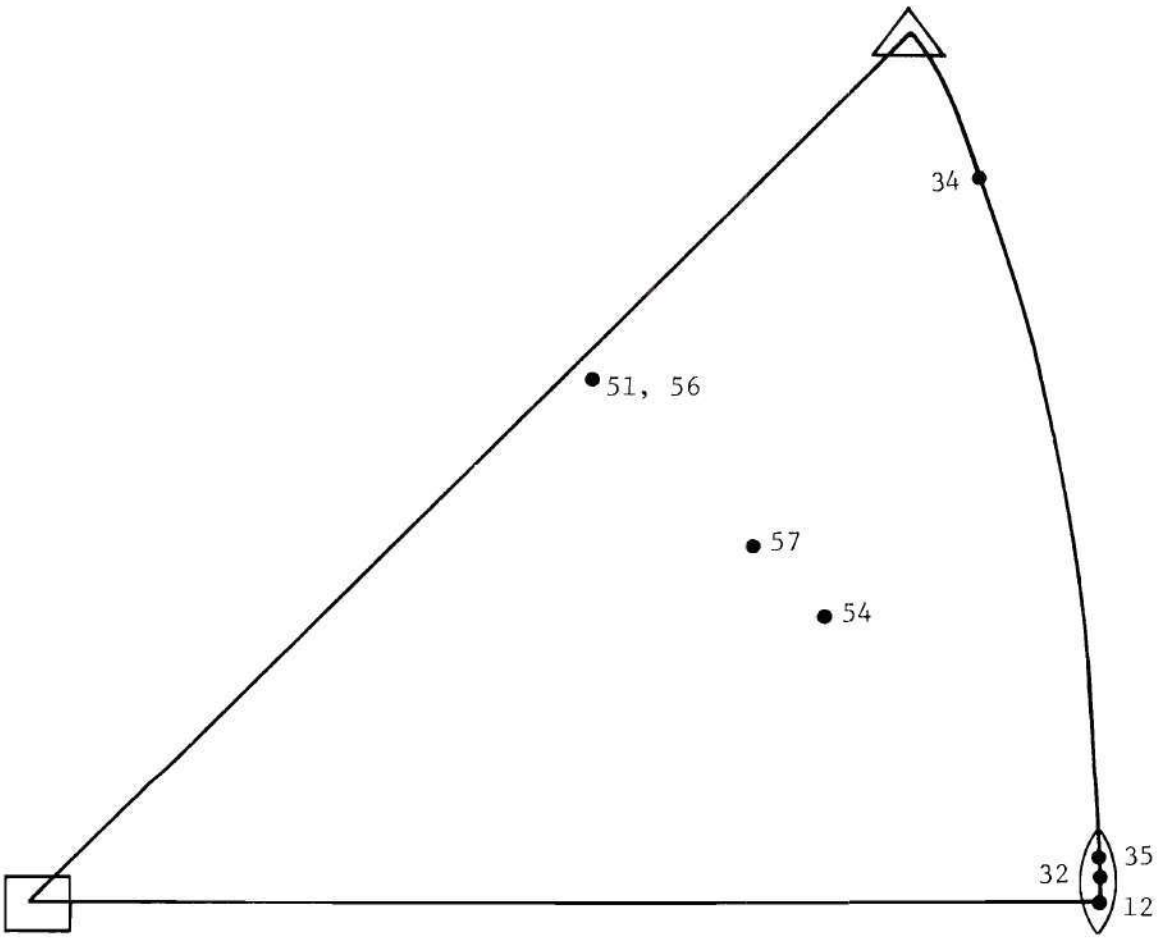

Figure 2. Orientation of Specimen Tensile Sets.

mm wide tab sections. Although samples of this geometry presented an uncertainty for calculations of resolved shear stress and strain, their use as a reproducibility check was unambiguous.

Following the high temperature vacuum anneal, epitaxial coatings were grown on the tensile specimen substrates by vacuum deposition at a pressure in the neighborhood of 2×10^{-6} Torr. A quartz frequency thickness monitor was used to fix a constant coating thickness of 2200 Å on both sides of each of the coated tensile specimens reported in these investigations. In addition, several copper single crystal tensile substrates were coated with nickel films of either 400 Å or 600 Å thick. The quartz frequency monitor thickness measurements were verified by analysis of the line widths in diffractometer scans according to the Sherrer Formula[47] for line broadening. Magnetic measurements were made on several Cu-Ni specimens taking advantage of both the well behaved magnetic properties of nickel and the availability of a sensitive automatic torque magnetometer.[48] Thicknesses computed from the film geometry, the measured magnetic moment and the bulk saturation magnetization[49] of nickel were consistent with the quartz frequency thickness monitor values. If there had been significant alloying at the Cu-Ni interface, the magnetic thickness would have been lower since copper added in solid solution to nickel rapidly and linearly lowers the magnetization. Deposition rates were between 7 and 11 Å/Sec and the substrate temperature was 300°C for several hours before and during deposition. Immediately following film deposition, the substrate heater was turned off. The composite samples were then attached to brass tabs using Eastman 910 adhesive for mounting on a microtensile machine.

Mechanical Tests

The mechanical behavior of the interface specimens were measured on a small force tensile machine designed for these studies. A detailed description of this apparatus and techniques for its use appears in Appendix B. Deformation forces were generated by an electrical coil positioned in the radial field of a large speaker magnet. The coil was attached to one end of a force arm assembly and one sample mount was attached to the other end. The core of a differential transformer was located at about the middle of the assembly. Four tungsten fibers provided a friction-free suspension for the entire force arm assembly. A programable power supply provided a coil current which produced the desired tensile force on a specimen and the free core differential transformer measured the displacement from which strains were computed. An x-y plotter recorded the load-displacement curves. Plots of resolved shear stress versus resolved shear strain were computed from the Schmid relationships using a Burroughs B-5500 ALGOL program. The critical resolved shear stress was computed from the value of the force where the force-displacement curve first deviated from the straight line which characterizes elastic behavior.

Microscopy

Following deformation, the tensile specimens were cut from their tabs and examined using both optical and scanning electron microscopy. Optical micrographs were made using a Leitz Metallux Microscope. The rotary stage of this instrument allowed measurements of the angle between the stress axis and slip traces. A Watson interference objective was available for measurements of slip band heights. The interference

objective was a Michelson interferometer[50] and a mercury vapor lamp was used as the light source. The resolution limit of this instrument was therefore about 0.15 micron. Background vibrations presented occasional problems with the long exposure times required for interferograms. The scanning electron microscope was a Cambridge Stereoscan Mark II.

CHAPTER IV

RESULTS

The results of mechanical measurements on eight sets of interface specimens are summarized in Table 1. The major surfaces of the specimens were parallel to the crystallographic planes indicated, with tensile axes as shown in Figure 2. The listed values of the work hardening coefficient, $\Delta\tau/\Delta\epsilon$, were measured from computed resolved shear stress versus resolved shear strain curves at 0.10 strain. The data are grouped as shown since meaningful comparisons of interface strengthening effects are made only between specimen within a single set. Set 54 is listed as having two subsets because it became necessary to process the indicated pairs separately even though all four specimens were initially co-directionally machined from a single wafer.

The resolved shear stress-strain curves for the specimen of set 51 are shown in Figure 3. The yield stress of the nickel and copper coated specimens were respectively 92% and 9% greater than that of the specimens having free surfaces. The direct load sharing capacity of the coating should have contributed less than 1% of the measured strength. Duplex slip developed as expected in the specimens having free surfaces and that coated with nickel. However, only single slip was observed in the copper coated specimen. The rotation of the stress axis corresponds to overshooting of about 2°. Measurements on another similarly oriented set (56), however, did not result in the large yield stress difference

TABLE 1

Summary of Results of Mechanical Tests on Interface Specimens

Sample Number	Coating	Plane	Stress Axis	CRSS (10^7 dyne/cm^2)	Work Hardening $(\frac{\Delta\tau}{\Delta\epsilon})$, ϵ=0.10
51 A	Copper	(111)	1° off [211]	8.80	3.3
51 C	None	(111)	1° off [211]	8.07	3.3
51 D	Nickel	(111)	1° off [211]	15.5	4.2
54 A	Nickel	(111)	14° off [211]	10.8	1.1
54 B	Copper	(111)	14° off [211]	7.39	1.4
54 C	Copper	(111)	14° off [211]	9.35	0.9
54 D	None	(111)	14° off [211]	7.39	1.5
56 A	Nickel	(111)	1° off [211]	7.95	5.4
56 B	None	(111)	1° off [211]	-	4.2
56 C	Copper	(111)	1° off [211]	7.19	4.5
57 A	Nickel	(111)	10° off [211]	9.98	2.7
57 B	None	(111)	10° off [211]	8.52	2.8
57 D	Cobalt	(111)	10° off [211]	11.1	3.8
12 B	Nickel	(100)	[110]	9.41	2.4
12 C	None	(100)	[110]	7.68	2.0
12 D	Copper	(100)	[110]	9.80	2.2
32 B	None	(110)	1.5° off [110]	5.95	3.5
32 C	Nickel	(110)	1.5° off [110]	6.74	3.3
32 D	Copper	(110)	1.5° off [110]	5.54	2.5
34 A	None	(110)	29° off [110]	5.74	3.4
34 B	Nickel	(110)	29° off [110]	7.37	6.5
34 C	Copper	(110)	29° off [110]	6.85	6.2
34 E	None	(110)	29° off [110]	5.78	7.2
35 A	Cobalt	(110)	3° off [110]	8.22	4.6
35 B	Nickel	(110)	3° off [110]	6.17	2.7
35 C	None	(110)	3° off [110]	6.35	2.2

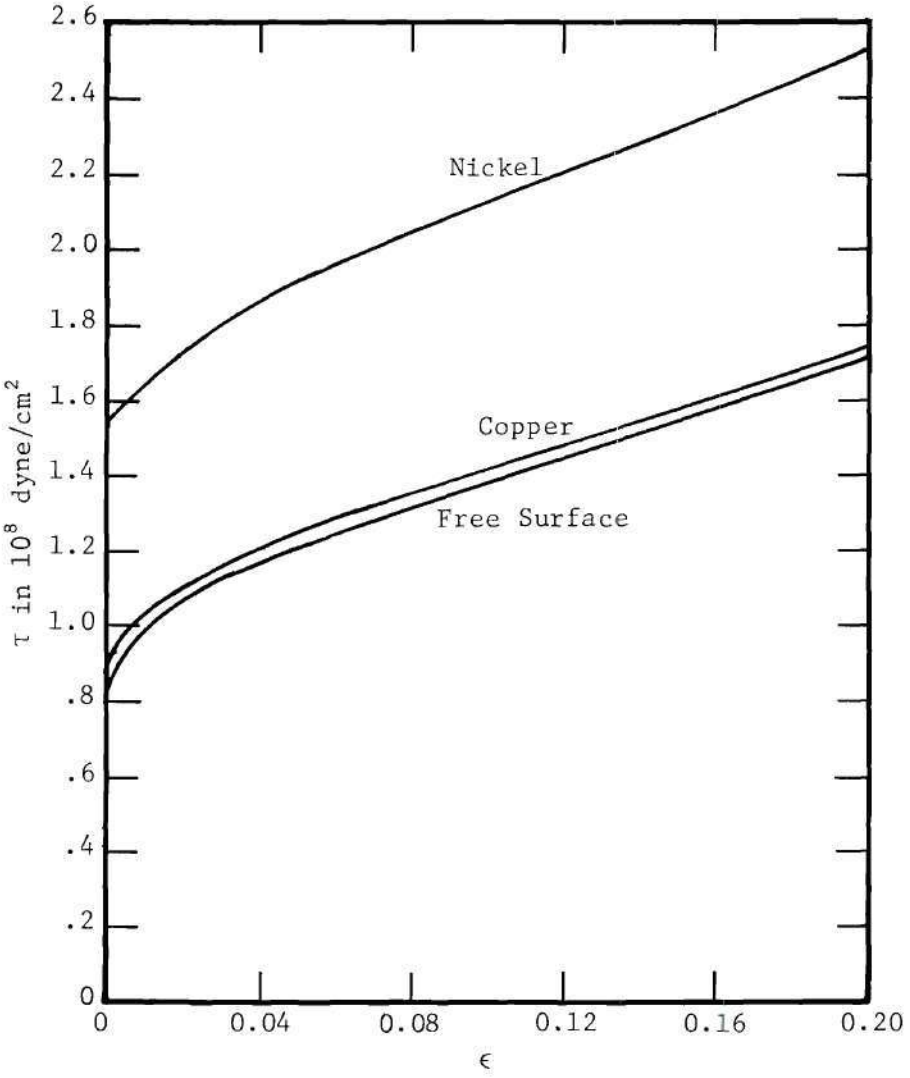

Figure 3. Stress-Strain Curves for Specimen Set 51.

noted above. The nickel coated specimen yielded at a resolved stress only 10% greater than that of a copper coated specimen. Unfortunately, the free surface specimen of this set was slightly bent during mounting so that its yield stress could not be determined. It was difficult to resolve slip traces on these surfaces using either optical or scanning electron microscopic techniques.

Similarly, Ni-Cu and Cu-Cu interfaces were grown on tensile specimens having (110) major surfaces. The stress axis of set 32 lay close to the (110) corner of the sterographic triangle where multiple slip is favored. The yield stress of the nickel specimen was only 13% greater than that of the uncoated specimen. However, the copper coated specimen had a yield point about 7% less than that of the uncoated specimen, and the work hardening coefficient of the copper coated specimen was somewhat lower than that of the other specimen of this set. The stress-strain curves for set 32 are shown in Figure 4.

Simultaneous activation of two slip systems was observed in each specimen during deformation. The scanning electron micrographs, Figure 5, show a herringbone appearance of the slip traces on the surfaces of the uncoated specimen. The orientation of the slip traces was consistent with that of the expected slip planes. An SEM micrograph of the nickel coated specimen at nearly the same magnification is shown in Figure 6. Although duplex slip is clearly evident, the herringbone structure did not occur in the central region of this specimen. As seen in Figure 6, most of the slip traces were long with discontinuous regions. Magnifications as high as 10,000X were employed to determine if this appearance was associated with a separation of the nickel film. Figure 7a shows a

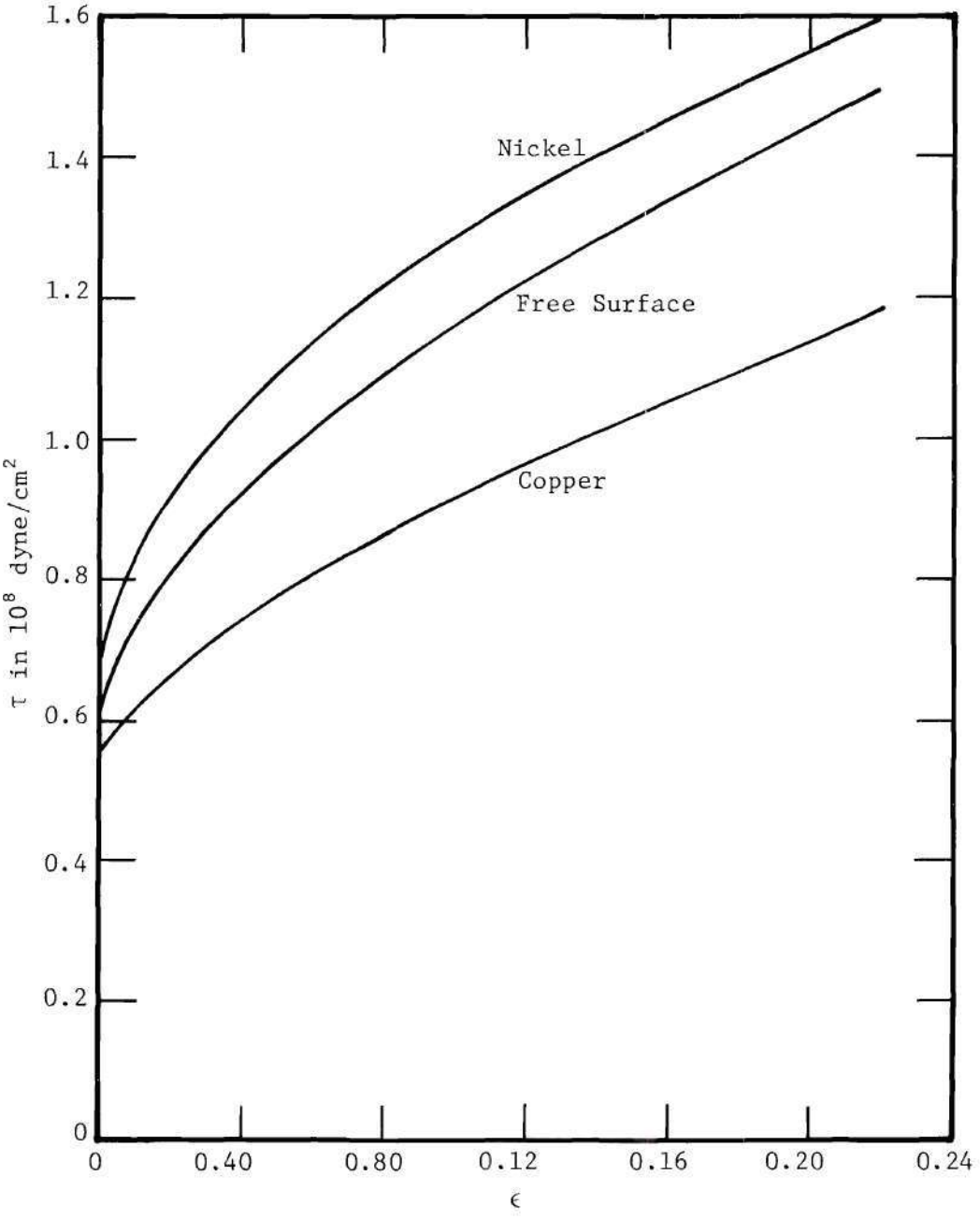

Figure 4. Stress-Strain Curves for Specimen Set 32.

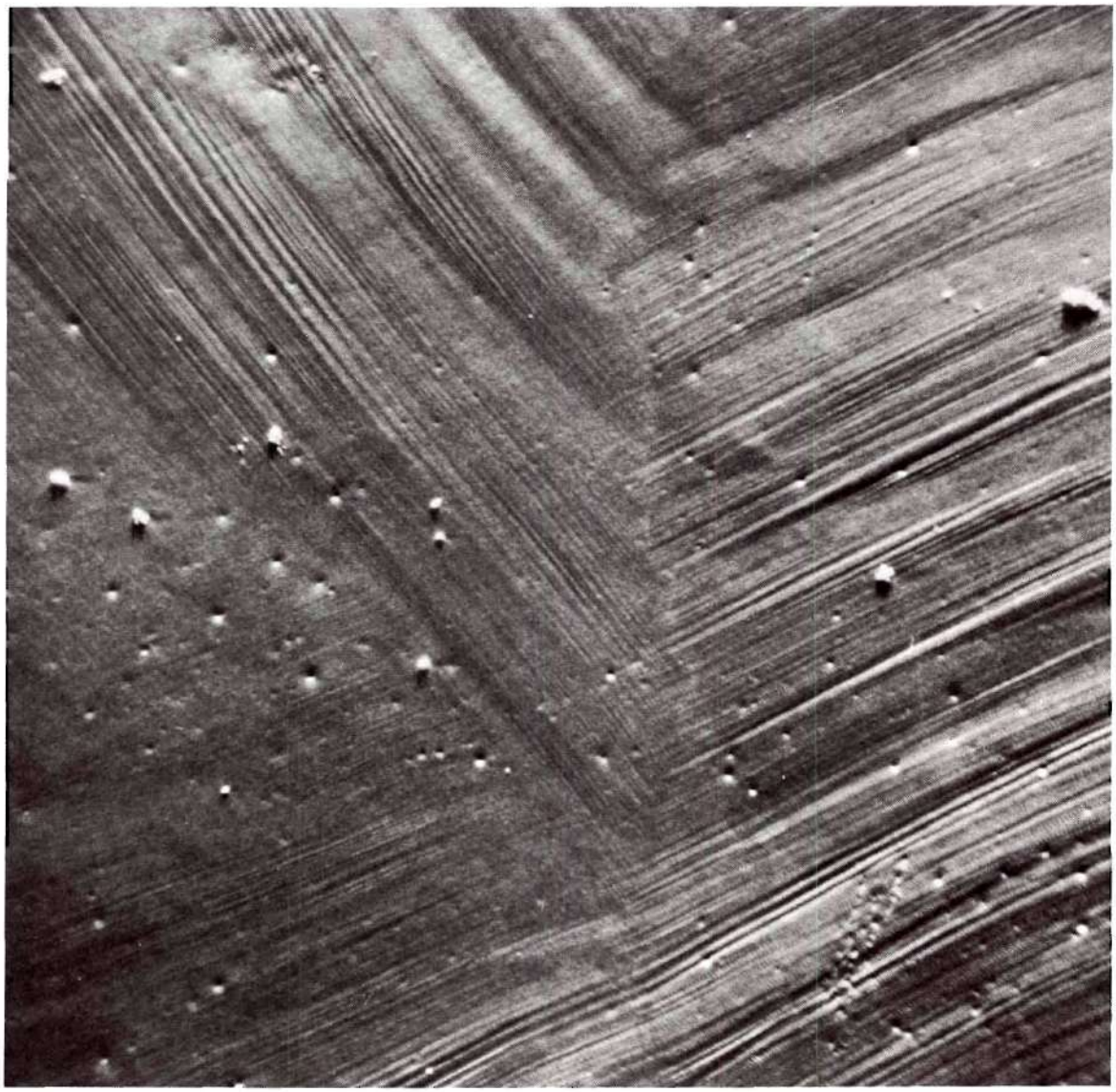

Figure 5. SEM Micrograph Showing Multiple Slip in Uncoated Specimen of Set 32. Magnification X130.

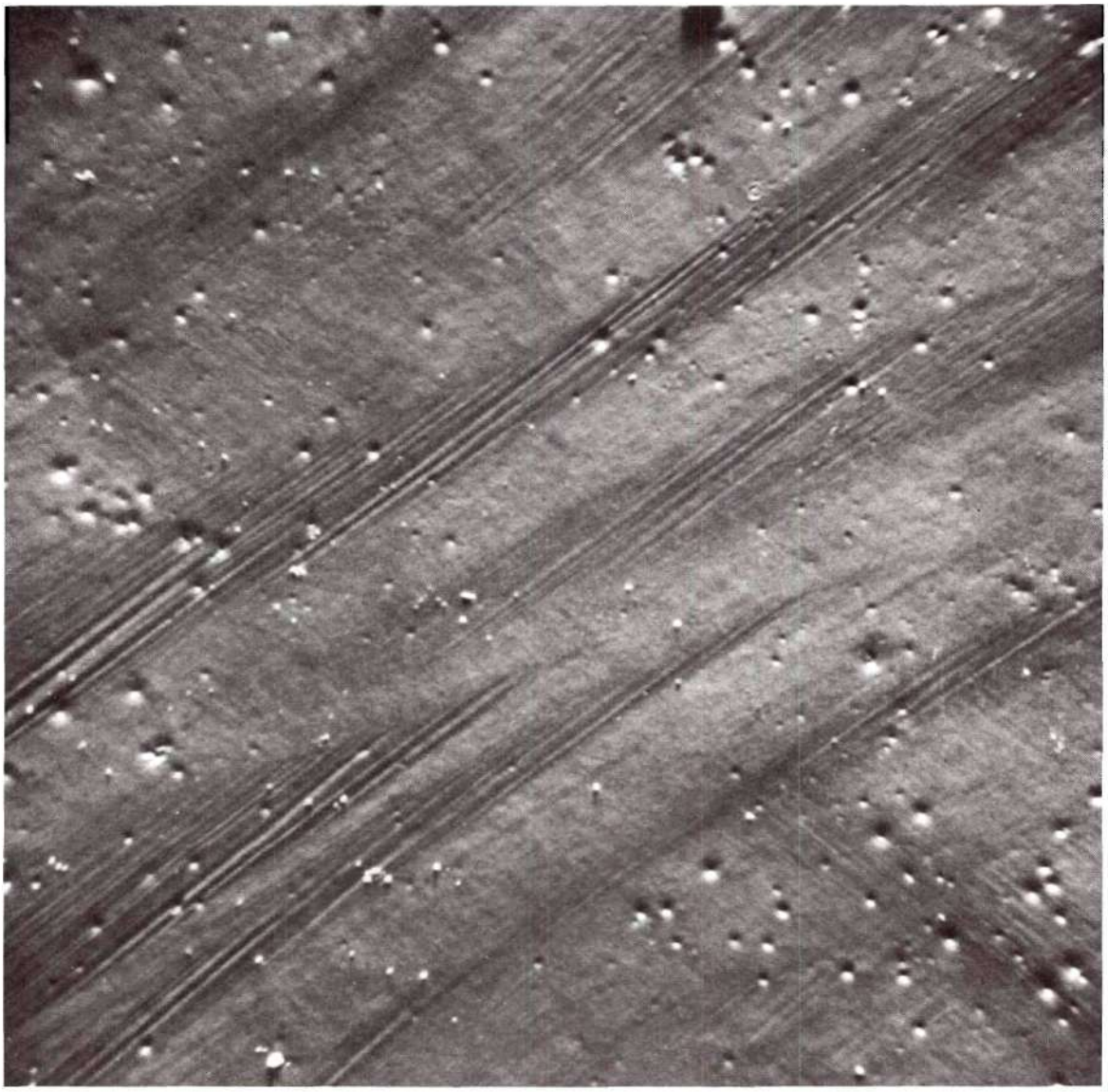

Figure 6. SEM Micrograph of Slip Traces in Nickel Coated Specimen of Set 32. Magnification X140.

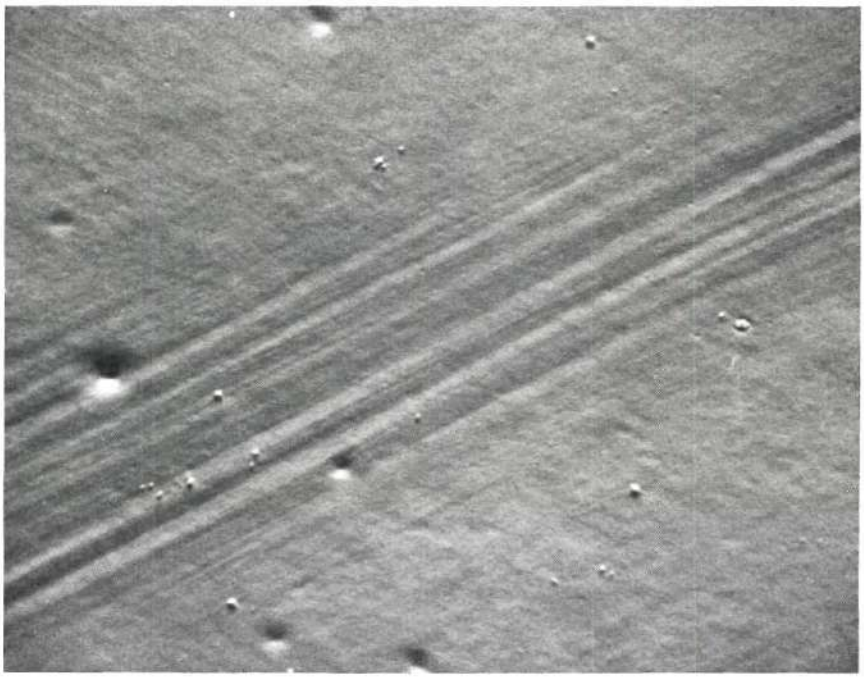

Figure 7a. Slip Traces Shown in Figure 6 at Magnification X520.

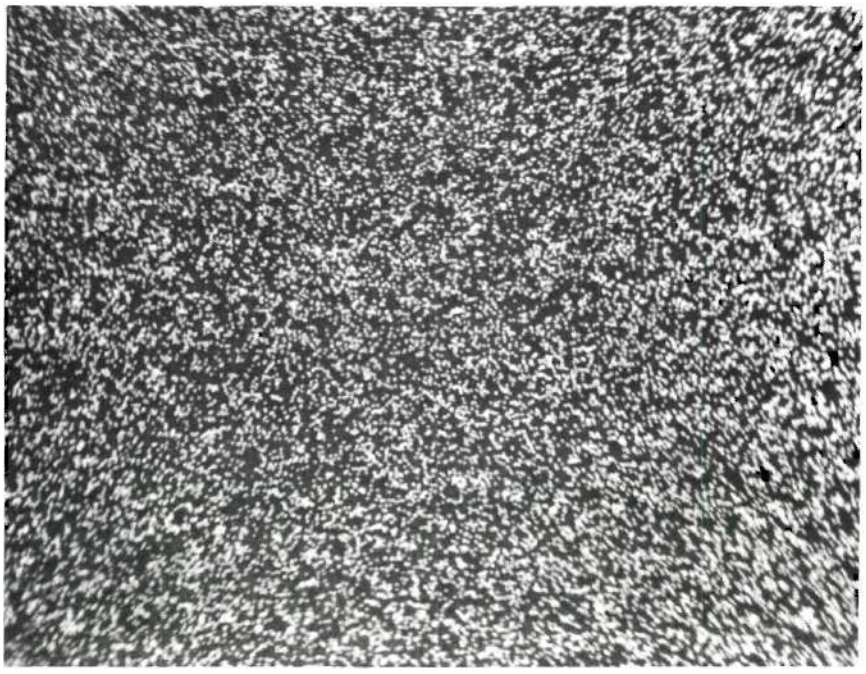

Figure 7b. Nickel X-Ray Fluorescence of Specimen Region Shown in Figure 7a. Magnification X520.

region of the specimen containing slip-trace-discontinuities at a magnification of 420X. The integrity of the nickel film is demonstrated in Figure 7b where the SEM electron beam was used to produce nickel x-ray fluorescence over the same area. No evidence was found which indicated coating discontinuity or fracture either in this or any of the other specimens employed in these investigations.

Micrographs of the copper coated specimen of set 32 were quite similar to those of the nickel coated specimen. An interferogram of the copper coated specimen appears in Figure 8 showing clearly the topography of the deformed surface. Apparent angles between active slip planes and the specimen surface as calculated from the interference fringes were generally much too small. Therefore, many of the apparently large slip steps were probably composed of uniformly spaced unresolved fine slip lines of heights somewhat less than 1000 Å.

Specimen set 34 had major surfaces parallel to (110) and was oriented with the stress axis somewhat near the [111] direction on the stereographic triangle. The resolved yield stresses for the specimen with a Cu-Ni interface and with a copper coat respectively were 29% and 19% greater than that of the two specimens with free surfaces. Although the yield stresses of the two free surface specimens agreed within 1%, their behavior subsequent to yielding was very different as is indicated by the listed work hardening coefficients. The specimen having the lowest work hardening coefficient also had a smaller thickness.

Micrographs of the specimens of set 34 were all quite similar to that shown in Figure 9. Bands of slip lines extended diagonally the

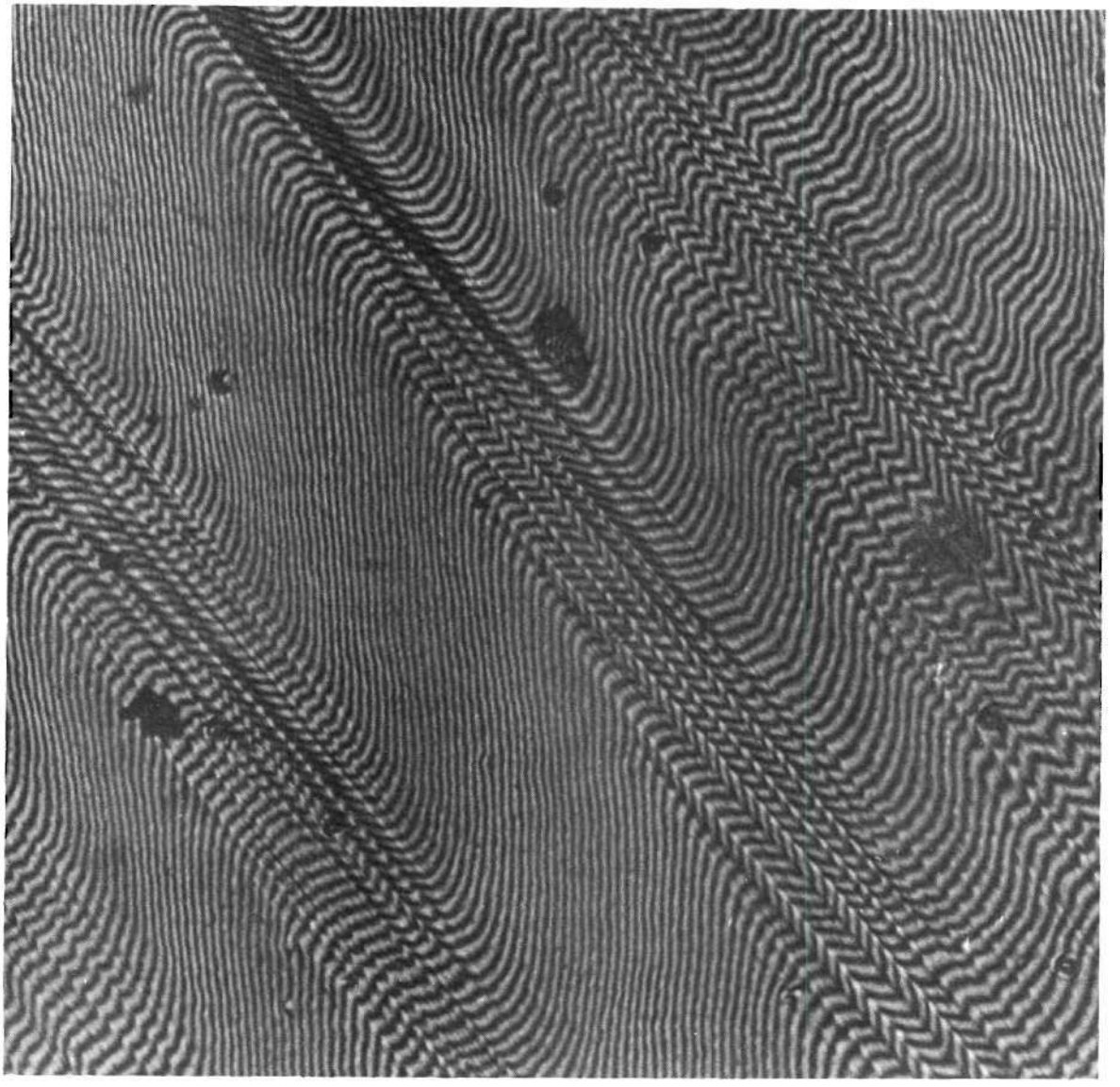

0.10 mm

Figure 8. Interferogram of Copper Coated Specimen of Set 32.

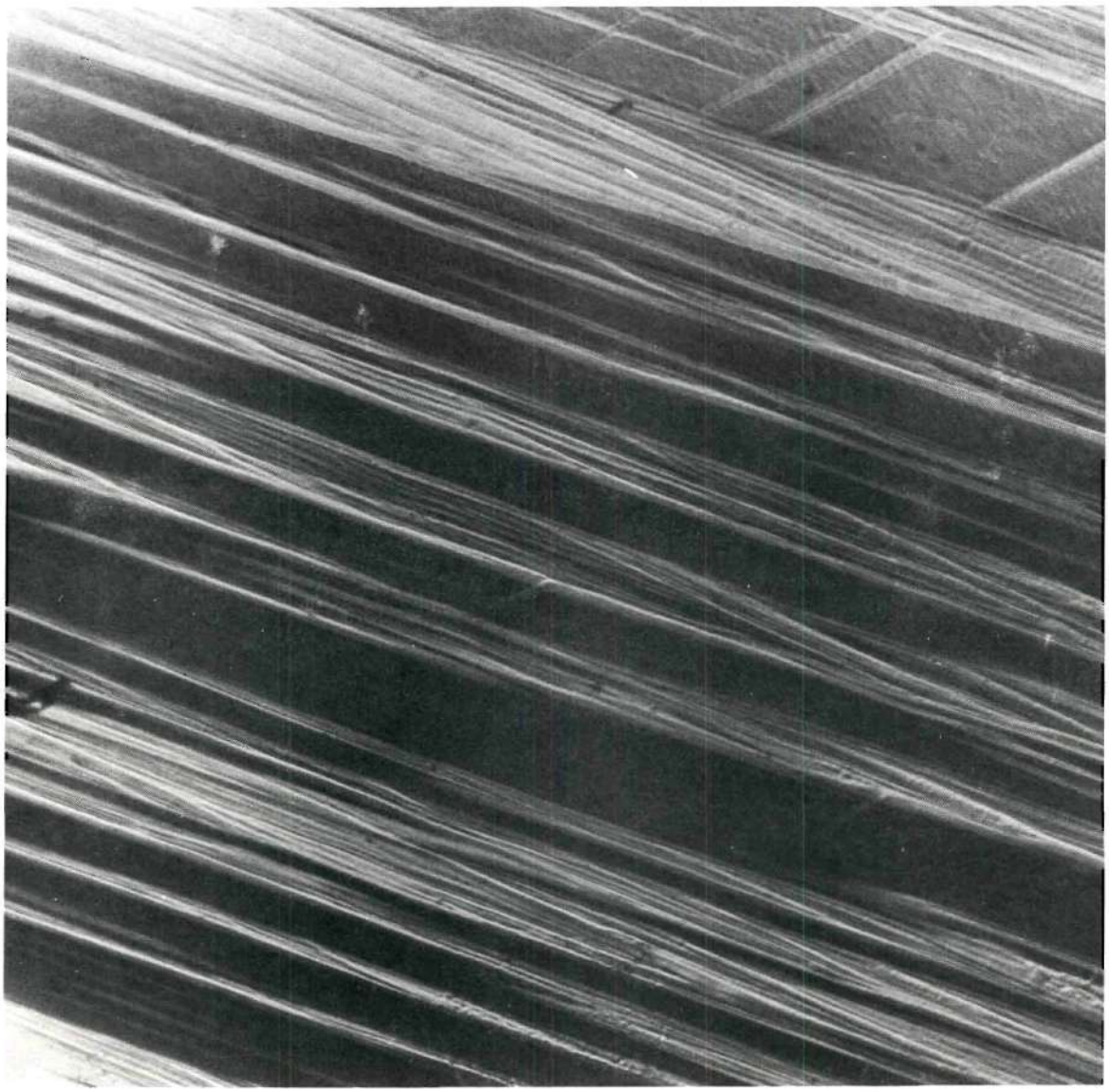

Figure 9. Optical Micrograph of the Nickel Coated Specimen of Set 34. Magnification X130.

full width of the specimen making an angle between 20-25° with the stress axis. The bands were separated by regions of relatively undeformed material occupying approximately the same amount of surface area as did the bands. However, the pattern seen in the lower part of Figure 9 with an appearance somewhat like ladder rungs, occurred in some regions of each specimen of set 34. An interferogram of a region containing "ladder rungs" is shown in Figure 10. Except for one free surface specimen, the work hardening coefficients of this set were two to seven times greater than values obtained with other sets.

Reliable mechanical behavior comparisons of set 54 can only be made within the pairs A-B and C-D for reasons discussed above. The orientation placed the stress axis near the center of the stereographic triangle and the major surfaces were (111). The resulting slip traces were very fine, parallel lines. The yield stress of the nickel coated specimen, 54A, was 46% greater than that of the copper coated specimen, 54B. The other pair resulted in a copper coated specimen yielding at a 25% higher CRSS than did the specimen with free surfaces. The work hardening coefficients, in the neighborhood of 1×10^8 dyne/cm^2, were considerably smaller than those of any other set.

Set 12 was oriented with major surfaces parallel to (100) and the stress axis at the [110] corner of the stereographic triangle. The nickel and copper coated specimens of this set had approximately the same increase in yield stress over that of the specimen with free surfaces, 23% and 28% respectively. Two slip systems were activated in each specimen.

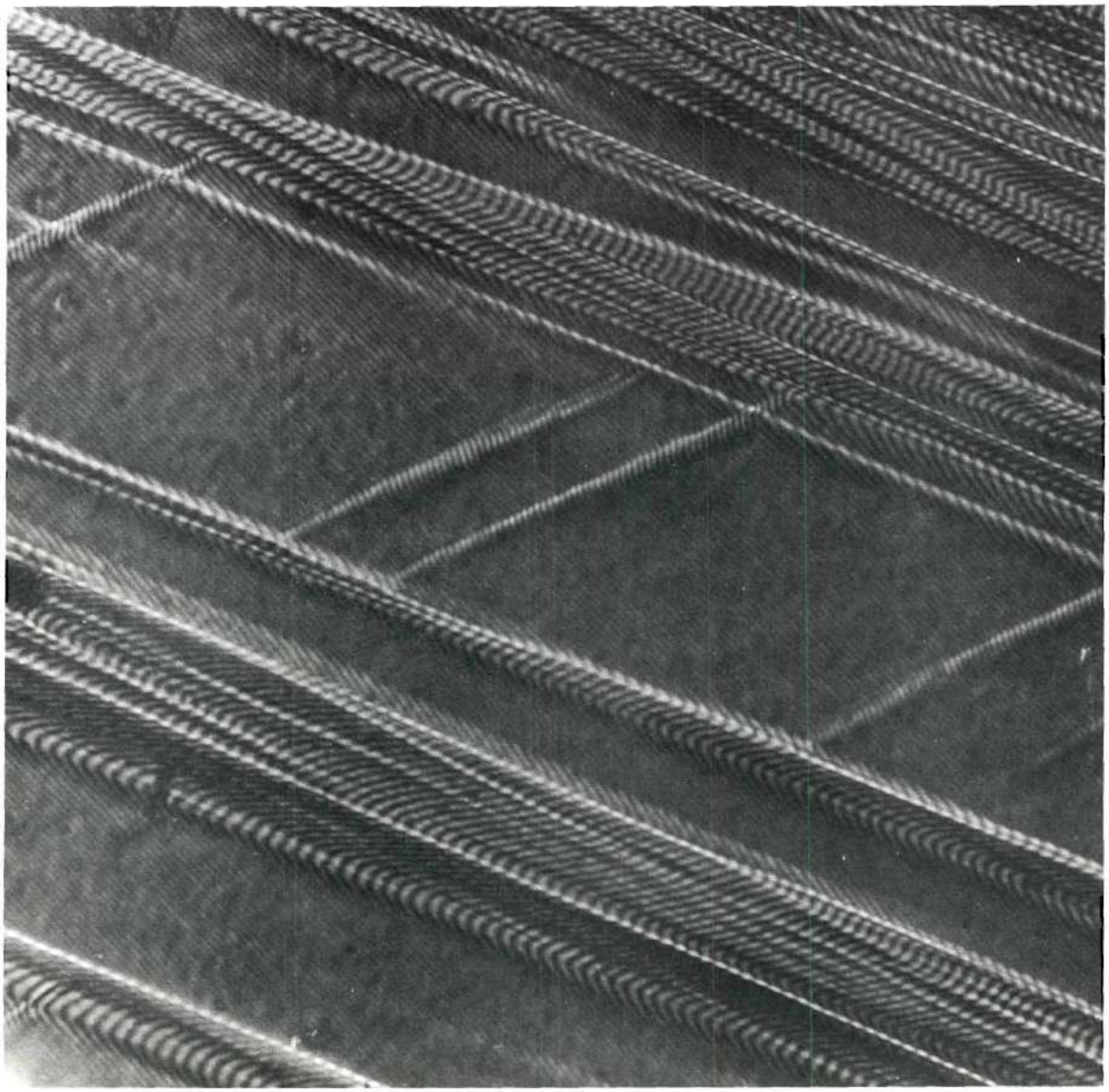

0.10 mm

Figure 10. Interferogram Showing Topography of "Ladder Rung" Structure in Nickel Coated Specimen of Set 34.

Cobalt layers were grown on tensile specimens of two sets, one having (111) and the other (110) major surfaces. Set 57, having (111) surfaces and oriented for single slip, resulted in cobalt and nickel coated specimens having respectively 30% and 17% increased yield stresses as compared to a free surface specimen. The stress strain curves for the specimens of this set are shown in Figure 11. A pronounced knee occurring beyond the yield stress is observed on the curve for the cobalt coated specimen and, to a lesser extent, on the curve for the specimen coated with nickel.

The orientation of set 35 was practically identical to that of set 32. The CRSS of the nickel coated specimen of set 35 was approximately equal to that obtained for the uncoated specimen as shown in Figure 12. However, the initial work hardening of the nickel coated specimen was somewhat greater than that having free surfaces and a knee again was apparent. The CRSS of the cobalt coated specimen is seen to be 30% greater and the work hardening coefficient at low strains was about twice as great. The multiple slip patterns which developed in the specimens of set 35 were all similar but complex as illustrated in Figure 13.

The macroscopic yield stress values of the thin specimens used in this study were somewhat greater than values generally reported in the literature for bulk copper single crystals. The preparation procedures required to produce such thin tensile specimens should undoubtedly be carefully considered for a possible influence in that processes such as radiation hardening, spark cutting and mechanical polishing are rather severe operations. The development of techniques for the

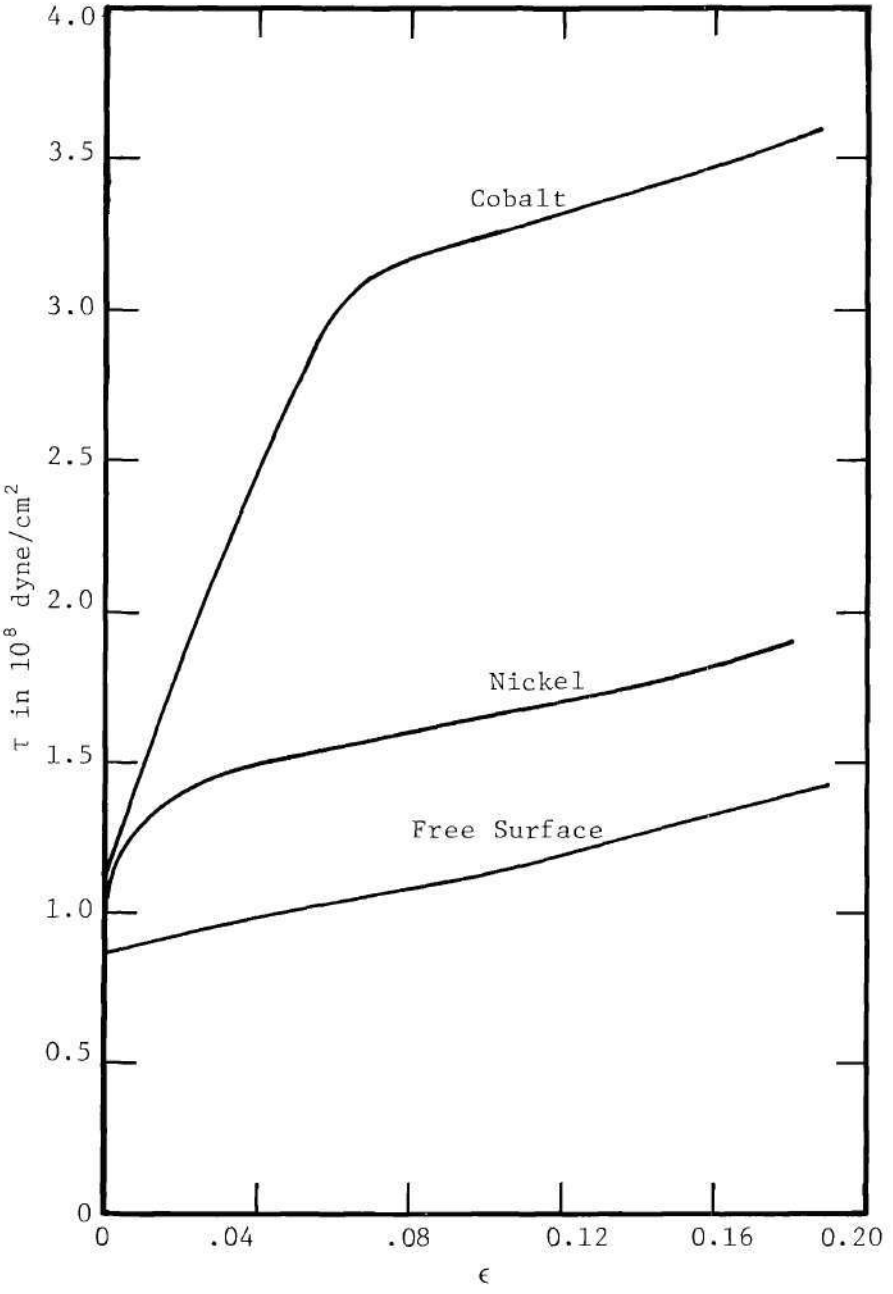

Figure 11. Stress-Strain Curves for Specimens of Set 57.

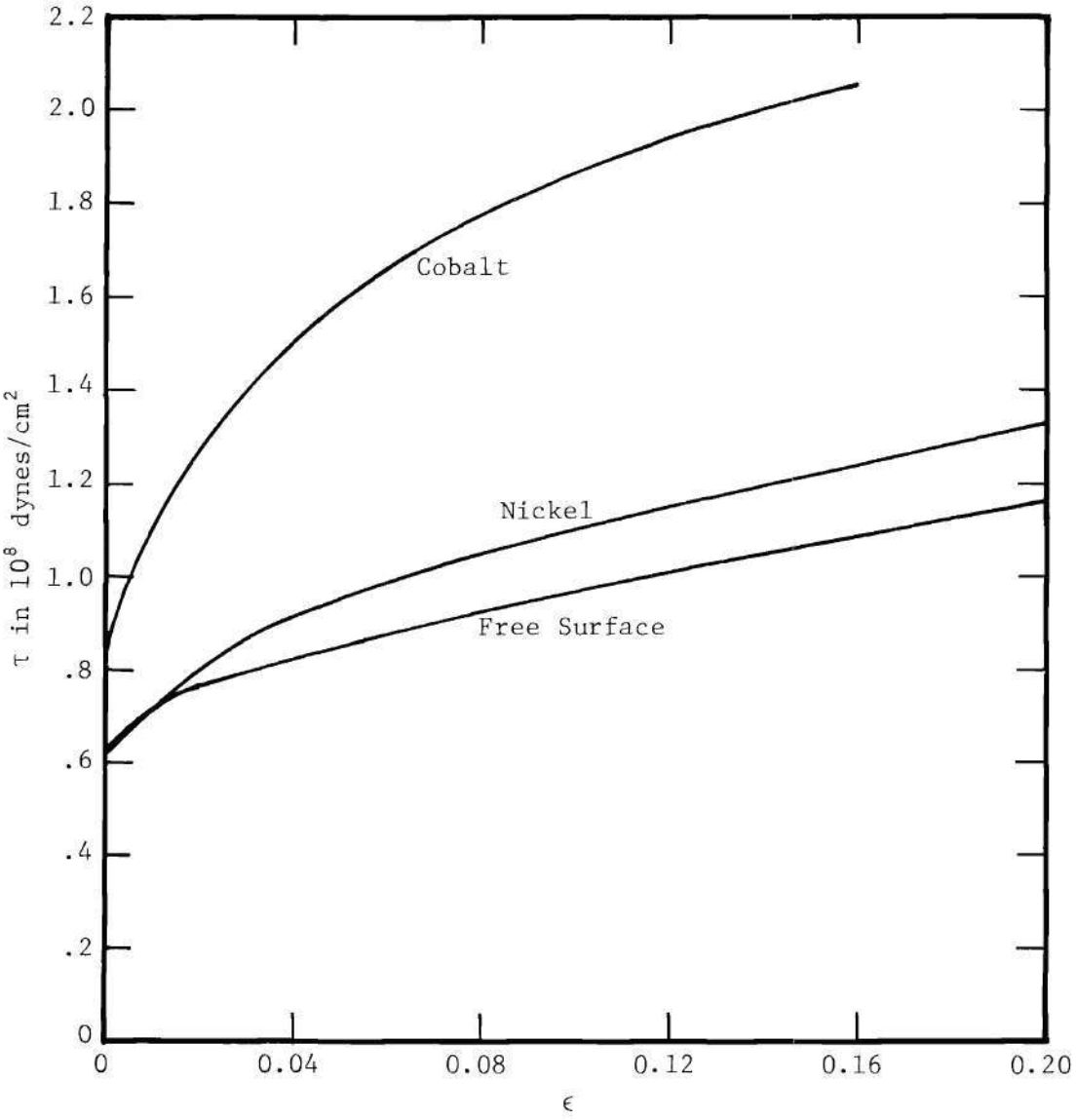

Figure 12. Stress-Strain Curves for Specimen Set 35.

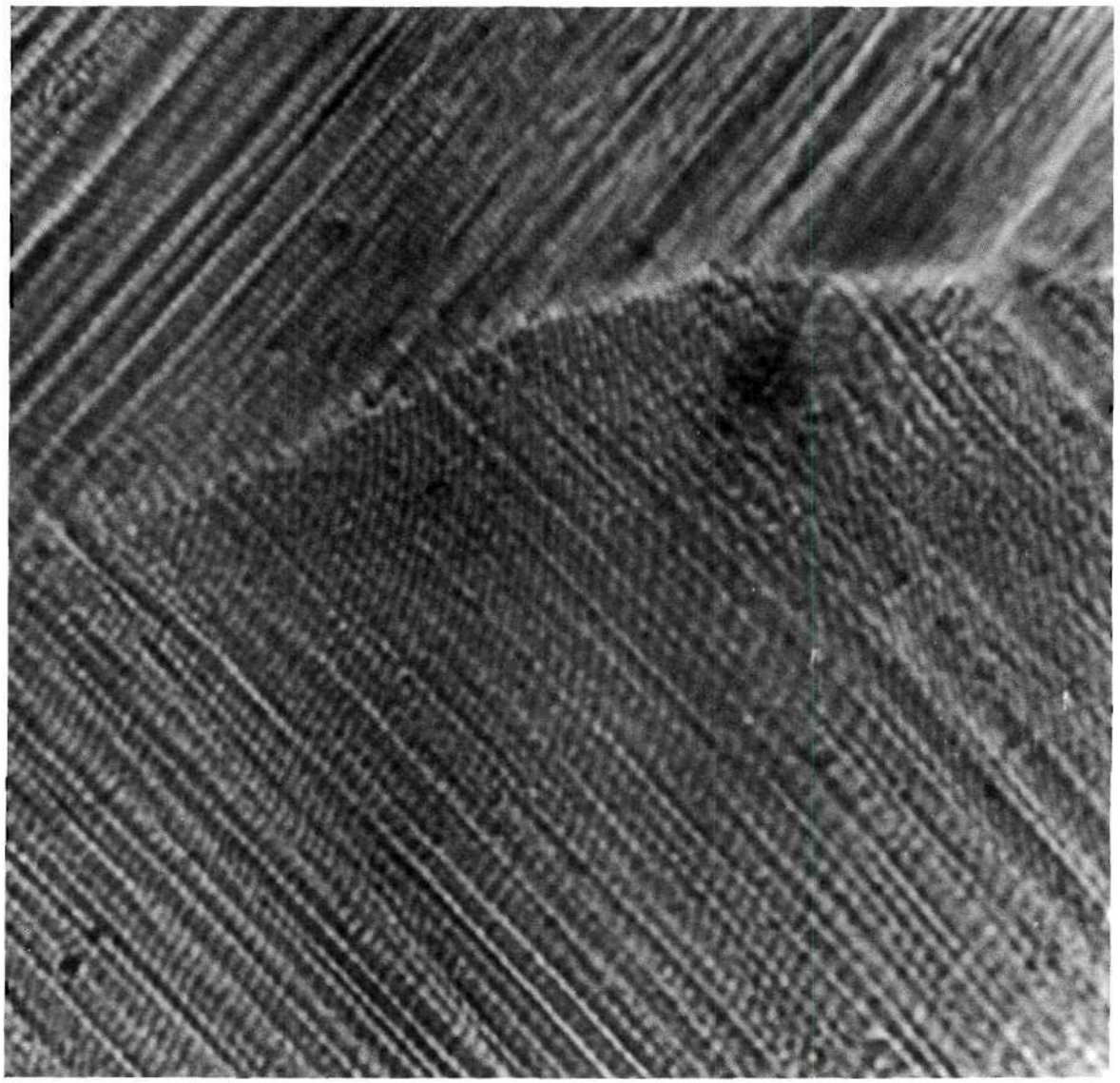

0.10 mm

Figure 13. Interferogram of the Uncoated Specimen of Set 35 Showing Topography of Multiple Slip.

production of thin, uniform single crystal wafers which do not require these steps is most desirable. However, high temperature vacuum annealing for different times and temperatures, even for values very close to the melting point, did not significantly alter the thin sample resolved shear stress values. In addition, Laue back reflection patterns of tensile specimens had well defined diffraction spots. Micrographs of etched wafer surfaces at one stage of the thinning process showed neither a second phase nor dispersions although low angle grain boundaries were occasionally found. It is therefore considered more probable that the range of yield stress values is somehow directly related to phenomena associated with tensile specimens having one dimension which is small.

During the course of these investigations, a number of tensile specimen were photo-machined from thin polycrystalline copper foils. These specimens were annealed in the same manner as those of single crystals, often at the same time, and similarly coated. The stress-strain curves obtained for polycrystalline tensile specimens having coatings of copper, nickel or cobalt were essentially identical. Even though the modulus difference probably influenced deformation within individual grains having exposed surfaces, factors such as the size and orientation of grains as well as grain boundaries resulted in the effects of a coating not being observable on a macroscopic scale.

CHAPTER V

DISCUSSION OF RESULTS

An interpretation of the observed strengthening effects requires an evaluation of the relative effectiveness of various interface factors. With one exception of small magnitude, interfaces between copper and either nickel or cobalt resulted in an increase in the critical resolved shear stress. The magnitude of strengthening was significantly greater than the simple load sharing capacity of the coatings. It also is significant that copper coatings usually increased the critical resolved shear stress, demonstrating the importance of considerations other than differences in material parameters at an interface. In no case did an epitaxial interface produce the significant weakening reported by Ruddle and Wilsdorf[21] for nickel plated copper crystals.

Even for the simple composite specimen configurations employed in these investigations, the probable dislocation interactions resulting in strengthening are numerous. The most important factors which must be considered may be grouped as follows:

1. Dislocation friction in the bulk material of the substrate.
2. Dislocation friction in the bulk material of the coating.
3. Coherency at the interface.
4. Impurities trapped in the interface.
5. Surface and interfacial energies.
6. Difference in elastic modulus.

7. Crystal structures of the components.

8. Crystallographic orientation of the specimen substrate.

Stress terms, τ_i, may be assigned to represent the contribution of individual factors where the subscripts, i, correspond to the order in which the factors are listed above. The total specimen stress, τ, may then be written as a superposition of the individual terms provided that cross interactions between the factors are negligible. The magnitude of the contribution from each factor will, in general, depend upon the physical and chemical parameters of the component materials, specimen geometry and preparation methods. Several of the stress terms were shown to be small for the particular interface combinations employed here. The sequence of measurements allowed particular terms to be evaluated by holding other contributions constant where their magnitudes either were uncertain or large.

Dislocation Friction in the Bulk Material of the Substrate

The measurements on preliminary single crystal specimens support the assumption that the bulk dislocation friction term, τ_1 is approximately the same for all specimen substrates of a single set. It then is possible to write $\Delta\tau_1 = 0$ for specimens within a set. The actual magnitude of τ_1 therefore is unimportant in a direct comparison of the mechanical effects associated with changes in other factors.

Dislocation Friction in the Bulk Material of the Coating

Dislocation friction in the coating material increases the strength of a composite specimen by two primary mechanisms. First, the coating material shares part of the load independent of other

interactions between coating and substrate crystals. Secondly, dislocation processes within a substrate are influenced by the friction encountered by a dislocation in the coating after traversing the interface. The defect density in a deposited coating is likely to be greater than in a substrate crystal so that the coating material has an effect somewhat like a work-hardened surface region. The "grown in" dislocation network inhibits the motion of the glide dislocations. The load sharing contribution was probably about 1% of the composite yield stress for copper coatings and about 2% for nickel and cobalt coatings based on coating dimensions and likely yield stress values. The strengthening associated with the second process is more difficult to estimate but, in any case, is likely to be of the same order of magnitude for the different coating materials within a single set. It, therefore, is probable that the contribution to the stress from the coating bulk, τ_2, is small relative to τ and that $\Delta\tau_2$ is very small for the *different coating materials* used here.

Coherency at the Interface

The choice of copper-nickel and copper-cobalt interface systems, where the lattice misfit is small, was designed to minimize strengthening effects associated with coherency. The primary coherency strengthening process for these systems should be due to the accumulation of residues as glide dislocations pass through the interface due to short ranged interactions between glide dislocations and the accommodating network.

The existence of accommodating networks has been predicted by theoretical treatments[26] although there is some controversy over their

existence at Cu-Ni interfaces.[24] Knowledge of the actual configuration and rigidity of either an accommodating network or a residue accumulation is required to estimate the magnitude of strengthening to be expected for coherency. Neither configuration is sufficiently defined to carry out a meaningful analysis but it is reasonable to assume that because the misfit is small for Cu-Ni and Cu-Co, the coherency strengthening effects are small. The coherency effect is certainly not the primary strengthening effect since specimens with Cu-Co interfaces had higher CRSS values than did those with Cu-Ni interfaces although Cu-Ni has a slightly greater lattice misfit.

Impurities Trapped in the Interface

Impurities consisting primarily of oxides and trace residues of preparation materials were probably present in the interfaces. However, the actual content was uncertain and, in any case, the amount present was very small. The effect of interfacial impurities on mechanical behavior was assumed to be about the same for all composite specimens of a single set since consistency was maintained in preparation conditions.

The mechanical tests on copper coated copper crystals provided some measure of the mechanical contributions associated with the combined effects of τ_2, τ_4, and part of τ_3. The coherency strengthening processes discussed above were associated with lattice misfit at the interface. However, coherency strengthening, τ_3, may occur at a Cu-Cu interface as well as, say, Cu-Ni due to the possibility for growth of tilt and twist boundaries at the interface between the copper coating and the substrate

crystal. As stated previously, the strengthening effect of both τ_2 and τ_3 should be small and positive. The CRSS values obtained for specimens having Cu-Cu interfaces were found to vary from set to set relative to that of corresponding specimens having free surfaces. However, the magnitude of the strengthening for a Cu-Cu interface on substrates having (110) or (111) major surfaces was shown to be significantly smaller than that of the corresponding Cu-Ni interface. The mechanical property variations noted between sets for Cu-Cu was probably due to small interfacial impurity differences in the different sets. This point is particularly evident in the behavior of set 12 where the Cu-Cu interface resulted in approximately the same increase in CRSS as did the Cu-Ni interface relative to that of the uncoated specimen. The preparation procedures were slightly altered for this particular set in that the length of time between the final electropolish and coating depositions were much longer than that of the other sets. Although the substrate surfaces maintained a bright appearance, much additional time obviously was available for the growth of oxides. The mechanical behavior of set 12 is therefore considered to have less significance than that of the other sets. The importance of interfacial impurities to dislocation processes was also noted by Fedorenko and Vincent[31] in their investigations of misfit dislocation networks at Cu-Co interfaces.

Surface and Interfacial Energies

The contribution of surface and interfacial energies to the sheer stress can be calculated as described in Appendix C. The load sharing contribution in the elastic region is approximately 700 dynes

for a copper tensile specimen having free surfaces and the geometry of specimens used in this investigation. This force corresponds to a tensile stress of about 5×10^5 dyne/cm^2 for the cross-sectional areas used here. An additional term results with plastic deformation because of the creation of new surface area as dislocations exit at the surface. The upper bound calculated for the effective surface energy contribution of a plastically deformed free surface copper specimen is approximately 2×10^6 dyne/cm^2. This value is only about one percent of the measured yield stresses.

A combination of surface and interfacial energies must be considered for a composite system. A dislocation passing from the copper crystal into, say, a nickel coating, generates new Cu-Ni interface area. New nickel-free surface area is generated as the dislocation passes on through and exits the nickel film. Appendix C shows that the maximum contribution from the combination of surface and interfacial energy terms is only about fifty percent greater than the value obtained for the deforming specimen with free surfaces. The surface stress abruptly drops to the free surface value as the slip step exceeds the coating thickness. The net surface and interfacial energy contribution, τ_5, is still less than two percent of the measured tensile yield stress. Contributions to the shear stress as a result of surface and interfacial energy changes with strain were therefore not sufficient to account for any major features in the stress-strain behavior of specimen used in these investigations.

Difference in Elastic Modulus

Interaction forces between a dislocation and a discontinuity in elastic modulus across an interface are governed by specific geometrical considerations as well as modulus values. The success of comparisons between theoretical and experimental results will therefore be determined by how closely a physical interface can be matched with a model for which calculations can reasonably be carried out. An approximation of the specimen interface geometry used in these investigations is provided by the simple model considered in Appendix C. The force acting on a single screw dislocation near a free surface varies inversely with the distance from the surface[5] and is directed toward the surface. Ignoring other factors, this behavior should also hold for a dislocation near a Cu-Cu interface, but with the dislocation distance measured from the outer surface rather than the interface.

The interaction forces calculated for a dislocation located at various distances, a, from interfaces between a copper substrate and 2000 Å films of nickel and cobalt respectively are plotted in figures 28 and 29. The force becomes repulsive for dislocations located within a distance of 500 Å of a Cu-Ni interface and 600 Å of a Cu-Co interface. The calculated interaction force becomes large as the dislocation is moved closer to the interface. However, calculations based on a linear strain field model are probably not meaningful closer than about 10 Å even for a perfectly planar and abrupt interface. At 10 Å, a repulsive force of approximately 50 dyne/cm, corresponding to a shear stress of about 2×10^9 dyne/cm^2, would be expected.

Force and stress values computed for 2000 Å thick nickel and cobalt films are tabulated in Appendix C for several dislocation

distances from the interface. Several conclusions may be drawn from results of these calculations: (1) the magnitude of the repulsive force is significant at least 300 Å into the substrate crystal, (2) a comparison between computed force values indicates that the modulus contribution to the CRSS for a cobalt coated specimen should be twenty percent to sixty percent greater than that for a nickel coated specimen, (3) the magnitude of the long range attractive force beyond the equilibrium point is a maximum at a distance about equal to the film thickness and is much smaller than that of repulsive forces occurring near the interface.

Values calculated for the repulsive force on dislocations near a positive, abrupt elastic modulus discontinuity indicate that the yield stress of carefully prepared specimens should be much larger than the experimental values obtained both here and elsewhere.[20-24] Details concerning the structure of the interface have a large bearing on the magnitude of the actual interaction. However, no assumption is made concerning the crystal structure of the coating material so elastic modulus strengthening effects require only that the coating adhere well to the substrate surface. Neither epitaxy nor a particular crystal structure was assumed and the coating material could even be amorphous. In addition, the development of cracks in a coating which otherwise adheres well to the substrate should not reduce the effect of a modulus difference greatly until the density of cracks becomes large. The long-ranged stress field of a dislocation interacts with large areas of the interface and the modulus effect should remain until cracks

occupy a significant fraction of the area. This point was noted experimentally by Roscoe[14] in his early work.

Departure from an abrupt interface should alter the strengthening contributions in that a gradual change in atomic concentration through the interface may produce finite gradients in both the elastic modulus and the lattice constants. Abbreviated theoretical treatments[13,24] indicate that both the modulus effect and coherency strengthening should decrease with gradients in these parameters and finally become negligible compared to the lattice friction for sufficiently small gradients. The experiments of Patterson and Greenfield[24] and of De Jonghe and Greenfield[23] have generally confirmed this behavior for metal composite specimen where interfaces were deliberately extended using controlled diffusion anneals. The "surface diffusion-zones" studied by these investigators involved interfaces of Cu-Pt[23], Cu-Ni and Cu-Au.[24]

The modulus strengthening effect calculations based on the single dislocation model of Appendix C indicates that values of CRSS for nickel or cobalt coated specimen should be significantly greater than those observed. However, the actual geometry of the interaction elements is much more complex. The presence of multiple dislocations drastically modifies the assumption of a linear strain field surrounding an isolated dislocation. Koehler[12] points out that the low stacking fault energy of copper permits a perfect dislocation to disassociate into a pair of partial dislocations separated by a stacking fault of width between 8b and 12b. He argues that the only significant interaction then is between the leading partial and the interface so that

the image interaction forces should be about half the values calculated for perfect dislocations. In addition, even the best polished metal surfaces are far from flat on an atomic scale. A dislocation approaching the region very close to an actual metal interface interacts with local interfacial areas which may have random orientations relative to that of the averaged interface plane. The large interaction force values anticipated in this region for a perfectly flat interface might be higher than that for an irregular surface.

The strengthening associated with a discontinuity in elastic modulus, τ_6, appears to be the primary contributing interface factor in observed values of $\Delta\tau$ for the Cu-Ni and Cu-Co interface system investigated here. Contributions from the other interface factors, τ_2 through τ_5, are, as shown above, not sufficient to account for the measured magnitude of $\Delta\tau$. It is not possible to be specific about the exact magnitude expected for τ_6 because of the uncertainties discussed in the previous paragraph as well as the lack of basic understanding of the short ranged interactions involving nonlinear core regions and the multiplicity of dislocations. The measured increases in CRSS, $\Delta\tau$, which may reasonably be attributed to the elastic modulus difference range from about 1×10^7 dyne/cm^2 to 5×10^7 dyne/cm^2 depending upon specimen orientations. These values correspond to the shear stress required to overcome image repulsion for a single perfect dislocation at about 300 Å from a Cu-Ni interface using the model of Appendix C. The difference between τ_6 for the Cu-Co and Cu-Ni model interfaces of Appendix C assuming the 300 Å dislocation position is about 2×10^7 dyne/cm^2. This value is remarkably, and perhaps fortuitously, close

to the measured differences of about 1×10^7 dyne/cm^2 and 2×10^7 dyne/cm^2 for the Cu-Co and Cu-Ni interfaces of sets 57 and 35 respectively.

The data of Patterson and Greenfield[24] for unalloyed Cu-Ni interfaces on two much thicker copper crystals provide values of $\Delta\tau \approx 1 \times 10^7$ dyne/cm^2 relative to their uncoated specimen. Thicknesses of their evaporated nickel coatings were stated to be 319 Å and 536 Å, but the substrate temperature during evaporation was not listed. Measurements on corresponding copper coated specimens were not reported, but the interfacial impurity effects were probably not too different from those of the current investigations. The image repulsive forces are somewhat smaller for these much thinner coatings. Their CRSS value corresponds to the image force on a perfect dislocation about 100 Å from the Cu-Ni interface of a 500 Å nickel coating according to the model of Appendix C.

Crystal Structures of Components

A difference in crystal structures at an interface can have a large impedance on dislocation transmission. Such effects were minimized here with the selection of interface materials. Both copper and nickel have stable fcc structures at all temperatures. Thin films of cobalt on copper crystals have a matching fcc structure during the early stages of growth, but with regions transforming to hcp with increasing coating thickness. With the transmission of large numbers of dislocations during plastic deformation, an increasingly larger fraction of the coating material is probably converted to hcp. During this phase of the deformation a long glide dislocation may encounter,

simultaneously, a high density of alternate fcc and hpc regions leading to the large work hardening coefficients measured for cobalt coated specimens. The subsequent decrease in work hardening noted in Figure 11 is probably a result of nearly complete conversion of the cobalt coating to hcp.

Crystallographic Orientation of the Specimen Substrate

The crystallographic orientation influences the deformation modes of the thin copper substrate crystals in the usual manner.[2] In addition, the influence of image interactions in these specimens would favor dislocation lines which tend to lie parallel to the major surfaces. For the specimen with (111) major faces, the Burgers vector lies parallel to the surface resulting in the observation of very faint slip traces in the micrographs of these orientations. The plastic shear strain therefore produces displacements parallel to the (111) interface plane but has components normal to the interface for specimen having (110) or (100) major surfaces. Screw dislocations should therefore have been primarily responsible for the deformation of specimen in sets having (111) major faces. The orientation of active slip systems in specimen having (110) and (100) major faces favored dislocations having an edge component. The largest values of $\Delta\tau$ attributed to τ_6 occurred in specimen sets 51 and 54 where the major surfaces were parallel to a (111) plane. This would indicate that a dislocation having $\vec{b}$ parallel to the interface (i.e. a screw dislocation parallel to the interface) experiences a stronger repulsive interaction than

does a dislocation having a primary edge component. However, the number of specimens measured is not at all sufficient to consider this point conclusive.

The orientation of specimen set 34 resulted in micrographs having the particularly interesting features shown in Figures 9 and 10. The appearance of the "ladder rungs" is quite similar to that of deformation twins.[51] Although deformation twins have been reported in copper single crystals only at cryogenic temperatures,[50,51] the orientation of set 34 is that found most favorable for deformation twining. Efforts to unambiguously determine if the "ladder rungs" were indeed twins were not conclusive. The interferograms of growth twins[54] have a characteristic pattern which differed from the appearance of those of set 34. However, the obvious differences in the manner of production of growth and deformation twins leads one to not draw a negative conclusion from this result. The fact that work hardening rates were much higher for this orientation than any other is also consistent with those of specimens which twin.

Relationships Between Various Interface Factors

The presence of an abrupt modulus discontinuity was found to be the primary interface strengthening factor in these experiments. However, as described above, contributions from many other possible interface factors were either avoided or minimized through the careful choice of interface materials and preparation conditions. For other material combinations or preparation conditions factors such as coherency,[17,22,23,24] solid solution hardening,[23,24] and crystal structures of the

components[22,25] are known to become major contributors under certain conditions. The integrity of a particular interface was also shown by Patterson and Greenfield[24] to effect the film's influence on mechanical behavior. The importance of interfacial impurities was emphasized by the strengthening effects of copper coatings in the current studies as well as others.[22] However, none of these effects were as significant in the present study as that due to modulus discontinuities.

CHAPTER VI

CONCLUSIONS

1. The elastic modulus difference provided the primary strengthening mechanism for copper-nickel and copper-cobalt interfaces. An abrupt interface, small lattice constant misfit and compatible crystal structures are required for this factor to play a dominant role.

2. Direct contributions from surface and interfacial energy terms were not significant compared to either the bulk strength of the specimens or to contributions from all other interface factors.

3. Measurements on copper-copper interface systems illustrated the importance of interfacial impurities on mechanical performance.

4. Crystal structure changes induced in cobalt coatings with deformation resulted in high work-hardening compared to copper-nickel systems.

APPENDIX A

SAMPLE PREPARATION

Single crystal tensile specimens were prepared employing the step sequence described below.

Radiation Hardening

The starting material was bulk copper single crystal rods (99.999% purity) about one inch in diameter. Sections having desired orientations were spark sliced from these rods and placed in the core of the Georgia Tech Nuclear Reactor. Fast neutrons introduce defects which pin dislocations and thereby minimize sample damage during subsequent preparation steps. After an integrated neutron flux of 10^{17}- 10^{18} neutrons/cm^2 was accumulated the crystals were placed in a hot cell for about three weeks to allow the activated copper isotopes to decay. Monitoring the decay provided a neutron activation analysis of the material which confirmed the stated purity level. A trace amount of cobalt introduced a minor inconvenience in that the long lived Co^{60} isotope required special disposal procedures for products of subsequent cutting steps. It was also found best to place only small volumes of copper in the reactor at one time to minimize sample heating. The radiation hardening was removed in a later vacuum anneal.

Orientation

Orientation of stock crystals for producing wafers with faces parallel to desired crystallographic planes was carried out using one or

more of several x-ray orientation devices which could be transferred directly to the spark machine. An orientation device convenient for aligning stock crystals using a diffractometer is shown in Figure 14. It allows rotation about the sample axis and the vertical. After locating the normal to a desired plane the variables are locked and a cut made parallel to the plane.

A particularly useful orientation device fabricated from an astro compass is shown in Figure 15. Sample orientation was made using the Laue technique. The useful feature of this device is its configurational convenience for precision spark cutting. A third device convenient for orientation adjustments by spark planing was a commercial goneometer supplied by the manufacturer of the spark machine.

Wafer Cutting

Single crystal wafers are produced by first spark machining a surface on an oriented stock section parallel to the desired crystallographic plane. To produce a thin wafer of uniform thickness required special procedures for the second cut. Attempts to spark slice a thin section from the stock failed as the spark process produced stresses which deformed thin slices and closed the gap.

This problem was solved by preparing several polycrystalline copper right circular cylinders with polished ends. A cylinder was then placed in the orientation device shown in Figure 15 and adjusted so that the cylinder base was parallel to the plane traversed by the wire tool of the spark slicer. After carefully indexing the position and orientation of the cylinder, it was removed and the end thoroughly cleaned with acetone. The oriented face of the stock crystal was mechanically and chemically

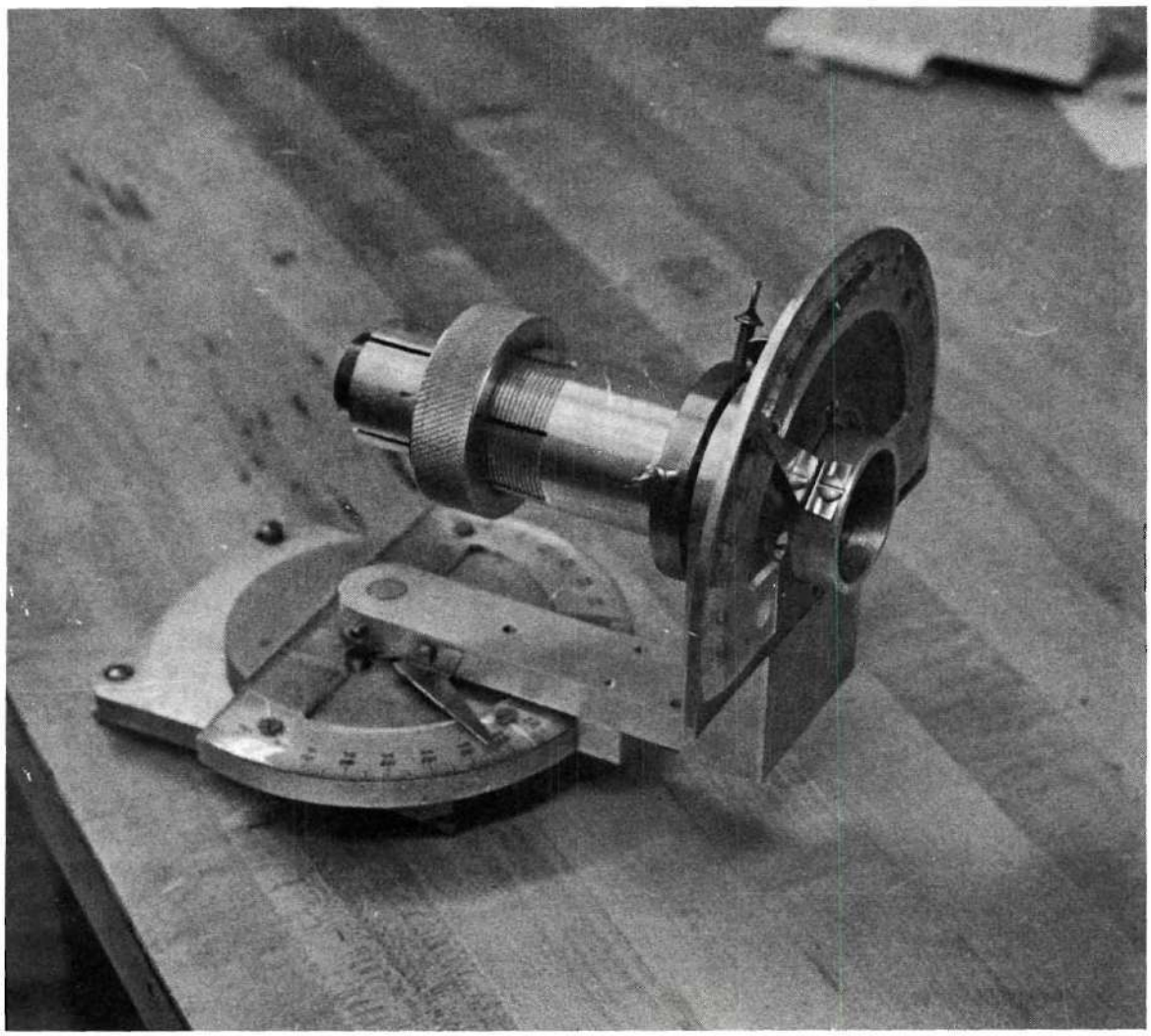

Figure 14. Orientation Device.

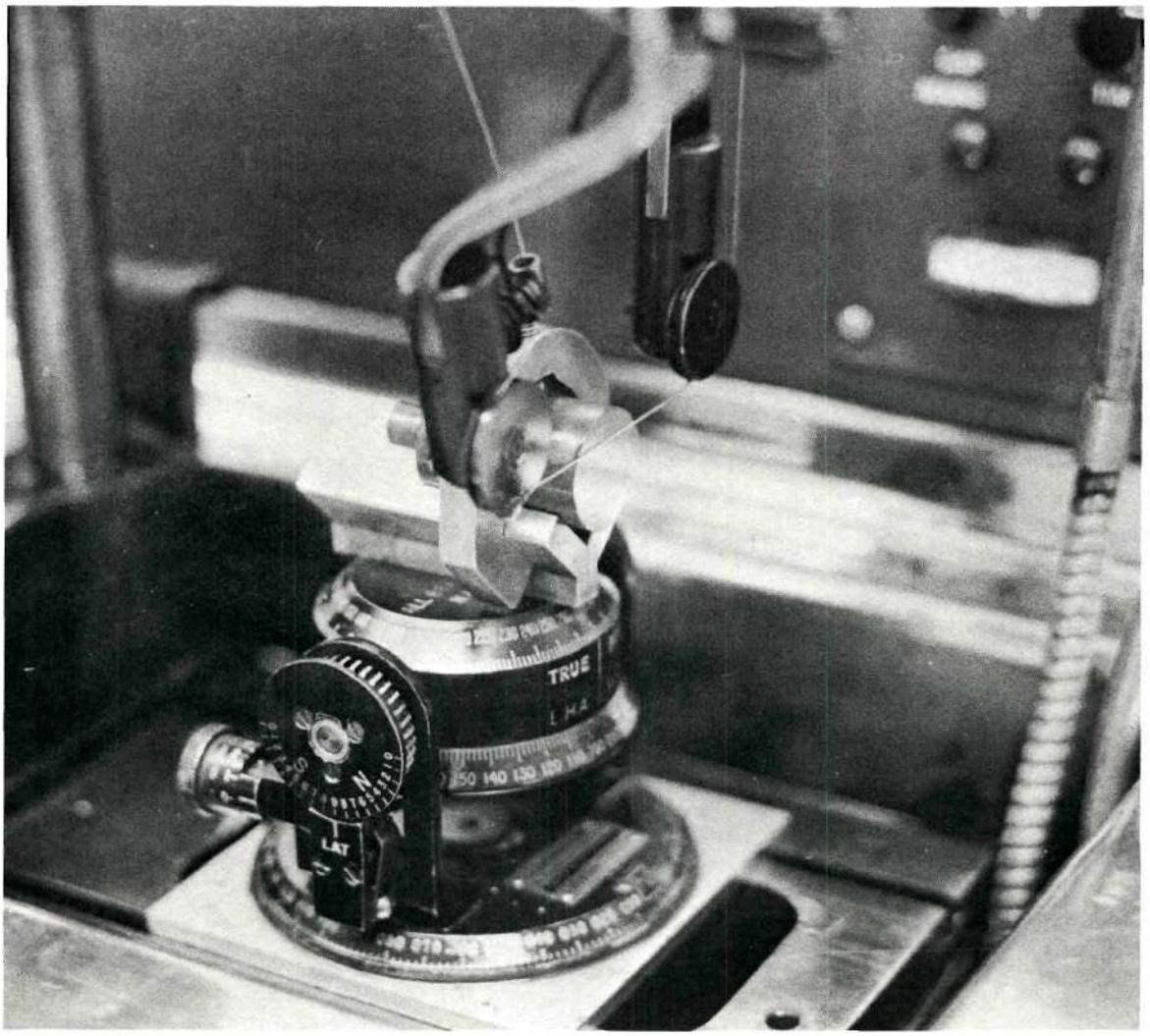

Figure 15. Sample Orientation Device Constructed From Astro-Compass Shown Mounted in Spark Cutting Machine.

polished and then cemented to the cylinder base using a uniformly applied film of Eastman 910 adhesive. It was necessary to remove excess adhesive in order to avoid spark insulation problems. After allowing about 10 minutes to insure that the adhesive was set, the cylinder with attached sample was returned to the position previously indexed and secured. A wafer of desired thickness was then produced by the spark slicer. Larger wafers were supported by polished brass plates cemented to the cylinder base.

An essential requirement for the production of large area slices of uniform smoothness was that a high volume, high speed jet of clear kerosene be directed into the cut to immediately remove all cutting debris. A special filtered circulation system satisfying the flow requirement was constructed. In addition, the filters conveniently collected radioactive waste products for prescribed disposal. Wafers cut in this manner had thicknesses ranging between 0.017 and 0.028 inch with variations less than 0.002 inch over the surface. The Eastman 910 bond electrically isolated the crystal but a spring clip completed the circuit. A cut wafer was separated from its support by boiling for a few minutes in di-methyl Formamide.

Wafer Grinding

It was desired to produce wafers about 0.005 inch thick whose opposite sides were parallel to the greatest degree possible before the final electropolish. Some success was achieved using standard precision spark planing procedures but better thickness control was obtained by mechanical grinding. Grinding blocks like that shown in Figure 16 were fabricated from a tool steel and hardened. They consisted of a solid cylindrical plug tightly fitted in a toroid. A set screw pressing into a side grove

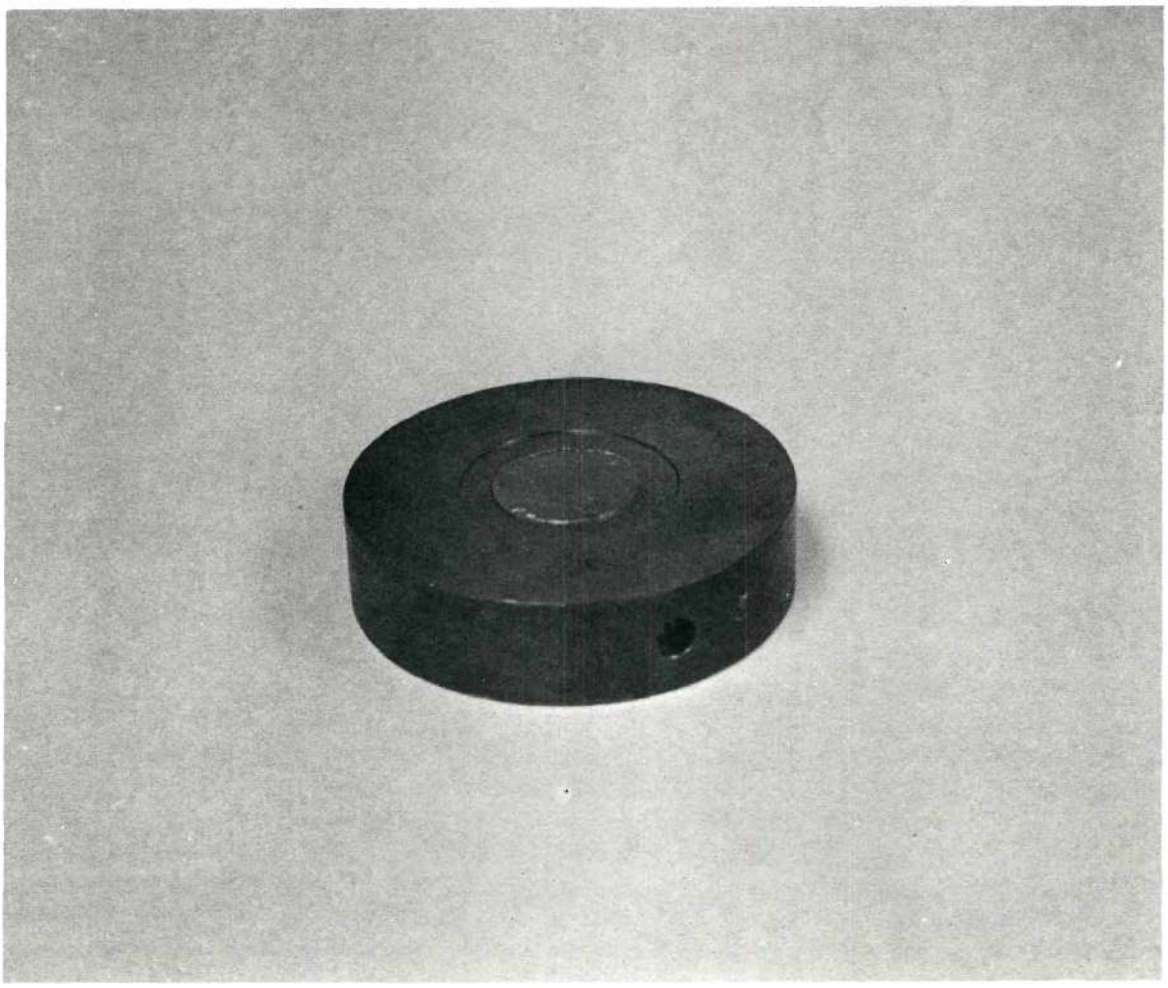

Figure 16. Wafer Grinding Block.

on the plug maintained rotational alignment and allowed the surface of the plug to be adjusted relative to that of the toroid. As required, the end faces of the hardened grinding block assembly were resurfaced using a precision surface grinder.

A wafer was uniformly thinned by first attaching it to the surface of the plug using either Pyseal wax or Eastman 910. Successive adjustments of the plug permitted material to be ground uniformly from the surface of a wafer in controlled increments. This process was repeated on the opposite face of the wafer to provide faces as parallel as possible. The last grinding step on each face employed 0.3 micron alumina.

The limitation on producing a 0.005 inch wafer of uniform thickness was usually determined by the uniformity of the adhesive applied between the block and the wafer. Pyseal wax was convenient since wafers could be quickly separated from the plug at a low temperature but Eastman 910 FS appears to be required for sufficient strength as a wafer becomes very thin.

Electropolish

Wafers were further thinned using a special electropolish cell arrangement. The electrolyte was a solution of 2/3 Orthophosphoric acid with 1/3 water. The wafer was suspended in the cell in a platinum wire cradle arranged so that electrical contact occurred only at or near the wafer edges. The periphery of a wafer was carefully coated with microstop using a hypodermic needle as a fine brush. Two cathode disks positioned on either side of the wafer were oriented so that planes of the cathodes and the wafer were parallel. The copper cathode disks were enclosed in pyrex cells having fritted glass on the sides facing the wafer.

Evolved gas passed out of the solution through pyrex tubes which supported the cells and enclosed the electrical leads. Bubbles and other debris forming at the cathodes were thereby prevented from reaching the specimen surface and interfering with the polishing process. This arrangement is shown in Figure 17.

The cell current and potential drop were monitored on an x-y plotter to provide a continuous reference of conditions relative to a previously determined "plateau" for optimum polishing. This proved to be particularly valuable as the cell had a negative resistance on the "plateau" and slowly drifted into a state where pitting occurred if timely adjustments were not made. After removing a sample from the electropolish cell it was thoroughly washed in distilled water and the microstop removed with acetone.

Success in uniform thinning was greatly affected by the cleanliness of wafer surfaces. Various standard techniques were employed for removal of adhesives, then adhesive solvents, oxides and unidentified contaminants. All components of the electropolishing cell were thoroughly cleaned and washed in distilled water prior to being mounted in the cell. During electropolish a magnetic stirrer was operated in the solution at a low rate. Since a wafer at this and subsequent stages was quite thin great care was necessary during handling to avoid mechanical damage. Even a misdirected stream of distilled water from a squeeze bottle could destroy a wafer or tensile specimen by bending. It was also essential that the surface be clean at each stage as even a trace of residue might either directly attack the surface or else interfere with a subsequent process and render a specimen set useless. The yield of useful specimen sets from satisfactory spark cut wafers was less than 30%.

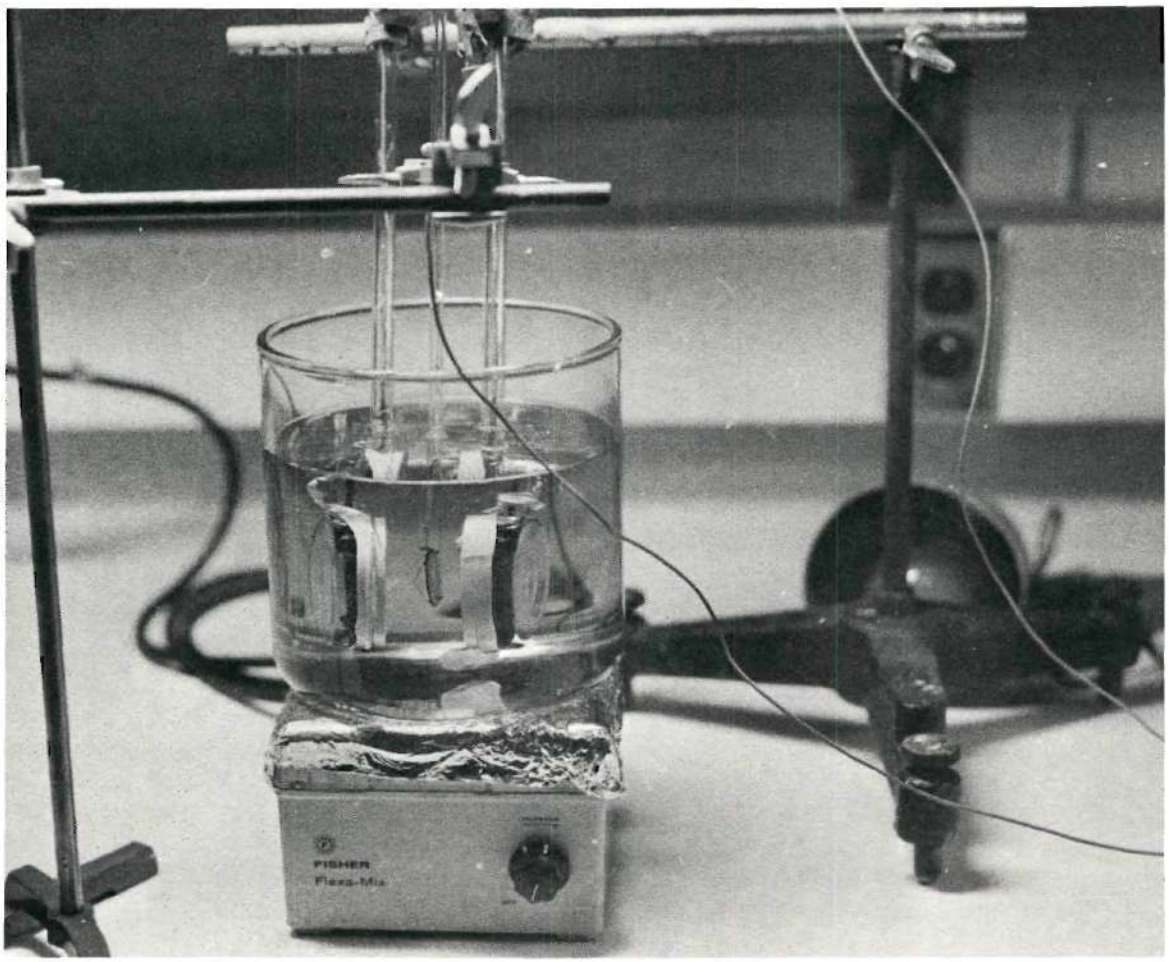

Figure 17. Electropolish Cell.

Photo Machining Tensile Specimen

Tensile specimens were machined from the electropolished wafers by employing photoetching techniques routinely used by fabricators of microcircuits. Following standard procedures, a mask was prepared having a number of identical and parallel specimen images with dimensions given in Figure 18. In this manner three or more tensile specimens having identical orientations were cut from a single wafer.

Even though the photoetching procedures are standard in the electronics industry, their application to forming single crystal tensile specimens was unusual. For this reason the step by step laboratory procedures adopted for this work are reproduced below.

1. Clamp the sample on an edge with metal tweezers, holding them closed with a paper clip.
2. Connect the sample and tweezers to the negative side of an electrocleaning cell. Run for about 3 minutes at 7-8 volts. Wash with distilled water.
3. Clean surface in HCl (10-40%) for about 30 seconds.
4. Rinse with distilled H_2O and alcohol.
5. Dry sample with hot air gun. Repeat steps (3) and (4) as necessary to remove lingering films from surface.

(Steps 6 through 9 are carried out under a dust free hood)

6. Suspend sample and tweezers in air above beaker of AZ-111 Photo-Resist, which is placed on an elevatable platform.
7. Raise beaker of AZ-111 until solution covers sample. Then lower beaker slowly, giving AZ-111 time to drain properly.
8. Dry the sample under IR lamp for 1-2 hours, turning several times.

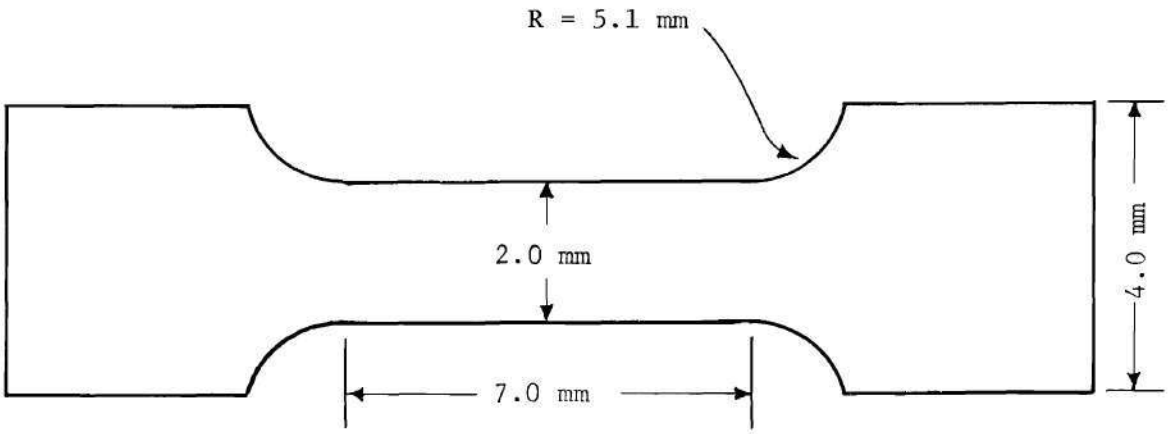

Figure 18. Tensile Specimen Configuration .

9. Cool sample to room temperature and load in press with mask and sample properly positioned.
10. Let sunlamp warm up for two minutes and expose sample for approximately five minutes.
11. Remove sample from press.
12. Develop in AZ-303 for $\sim$ 1 minute. (Note that the AZ-303 must be diluted 4-1.)
13. Etch sample in agitated ferric chloride until the copper is eaten away in the proper places.
14. Remove remaining AZ-303 with acetone.
15. Thoroughly wash tensile specimen in distilled water to insure that the etch solution is entirely removed.

Notes

A 275 watt sunlamp should be about 12 inches above the press during exposure. A 250 watt IR lamp should be about 7 inches above the sample, which should be over but not contacting aluminum foil. AZ-111 and AZ-303 are supplied by Shipley Co., Inc., Newton, Massachusetts.

Vacuum Anneal

Immediately after the tensile specimens were machined detailed dimensional measurements were made on each specimen and recorded. Precise optical measurements were made using a microscope equipped with a Cooke AEI Image Splitting Eyepiece. A low force dial gauge capable of resolving 0.0001 inch was also used for thickness measurements.

The sample set was then placed in the specially constructed high temperature vacuum anneal furnace shown in Figure 19. A sample set rested

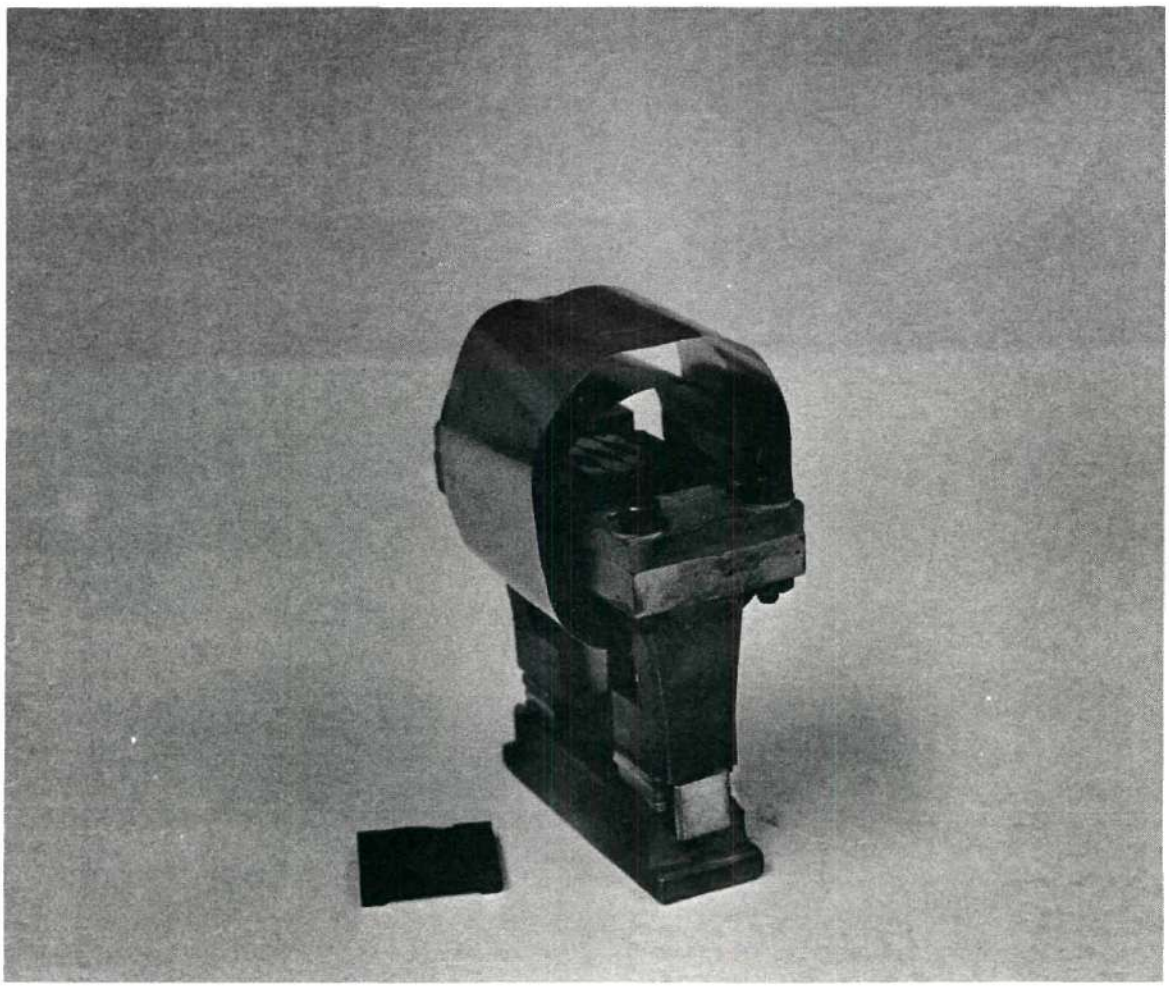

Figure 19. High Temperature Vacuum Anneal Furnace. (Part of radiation shield is removed to show interior.)

on a flat high purity graphite plate heated by a high current through a tantalum strip which supported the graphite plate. The temperature was monitored by a Pt-Pt 10% Rh thermocouple inserted into a hole in the graphite plate. A double radiation shield surrounding the sample area allowed the furnace to easily achieve 1200° C at pressures of 1x 10^{-6} Torr and less. Additional graphite flats having short legs at each corner permitted several sample sets to be stacked in the furnace at one time.

Most sample sets were annealed at temperatures between 750° C and 850° C for about 12 hours. Annealing close to the melting point of copper sometimes resulted in thermal etching so lower temperatures were used subsequently. Following the high temperature anneal, a Laue pattern was made of one specimen from each set for final definition of plane and stress axis orientation.

Film Deposition

Samples to be coated with a metal film were placed in a graphite specimen support block which fitted to a rotating shaft located in a substrate heater. A mask permitted film deposition on only the gauge section and immediately adjacent tab areas. The metal source material was placed in an Al_2O_3 coated tantalum boat located directly below the specimen support block. The arrangement is shown in Figure 20. With the specimen support block rotated so that an edge faced the boat, the source material was melted and outgased. Each side of a specimen was then exposed to the source for film deposition. The thickness was monitored using a resonating quartz crystal thickness device calibrated previously for the particular sample-source-crystal monitor configuration employed here. The output of the thickness monitor was recorded to provide a

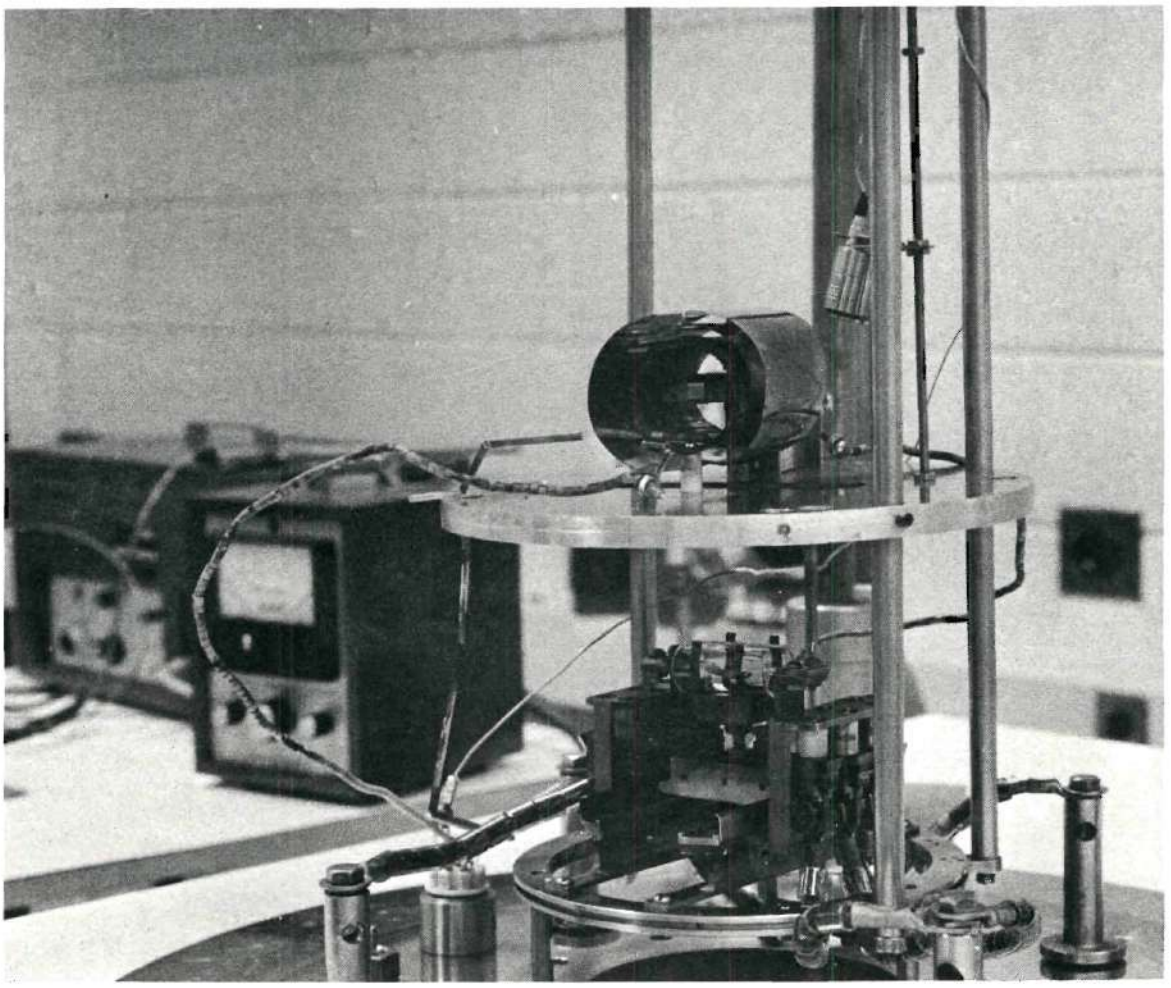

Figure 20. Vacuum Deposition Arrangement. (Showing rotating specimen holder inside heater directly above boat. The quartz crystal thickness monitor head is located at upper right of specimen heater.)

permanent record of detailed deposition rate. In this manner, films of essentially the same thickness were deposited on each face of each specimen. Film thickness was later verified using other techniques.

The specimens were maintained at 300^{0} C for a few hours prior to and during film deposition by means of the substrate heater surrounding the specimen support block. Following deposition the heater was shut off to minimize diffusion. These particular conditions were found to result in adherent epitaxial films grown on the specimen as verified by diffractometer scans.

APPENDIX B

MICROTENSILE INSTRUMENTATION

Introduction

The delicate nature of very thin samples requires special procedures for meaningful mechanical property measurements. The usual methods for measuring stress-strain characteristics may be divided into two major classes depending upon how the specimen is deformed. In one case a specimen is deformed by displacing one part relative to another with the machine supplying whatever force is required to provide the desired displacement. The displacement is most easily achieved using a screw driven crosshead with the resulting load on the sample measured with a suitable force transducer. In the second class a sample is stressed by the application of desired load levels and the displacement is then measured passively.

The large variety of machines employed in mechanical property measurements is generally well known so that a review is not necessary here. Although standard bulk sample testing machines may sometimes be modified to accommodate measurements on samples having small cross-sectional areas, their use for such pruposes is generally cumbersome. Accurate measurements using a screw driven machine require an extensiometer across the specimen to avoid displacement corrections associated with such factors as backlash in the screw mechanism and the motion necessary to actuate a load cell transducer. The force required to

actuate standard extensiometers is often a significant fraction of the deformation loads of thin samples. Special techniques for testing of thin samples have been reported.[54-56] The instrumentation system dessribed here provides a particularly convenient and versatile precision measurement system for investigations involving samples which either are intrinsically thin or which are made thin for a particular purpose. The second class of testing machine described above was found to be best suited for delicate sample measurements. The configuration adopted provides an automatic recording test system which allows mechanical property investigations involving environments ranging from corrosive liquids to ultra high vacuum.

Mechanical Design of Microtension Apparatus

A diagram of the force arm assembly is shown in Figure 21. A force coil is positioned in the radial field of a large speaker magnet at the left and one sample mount is attached to the right end of the force arm. The entire assembly is suspended freely by four 0.0015 inch diameter tungsten fibers with clearance in the magnet gap and differential transformer coil so that no friction occurs. A direct current in the coil therefore produces a force at the sample which is absolutely determined by the magnitude and direction of the coil current. The fibers have sufficient length so that except for very small force levels no correction is required for displacement of the pendulum from equilibrium. The differential transformer at the center of the assembly measures the displacement from which strain is determined.

The force coil is wound on an aluminum coil form 1.25 inch long

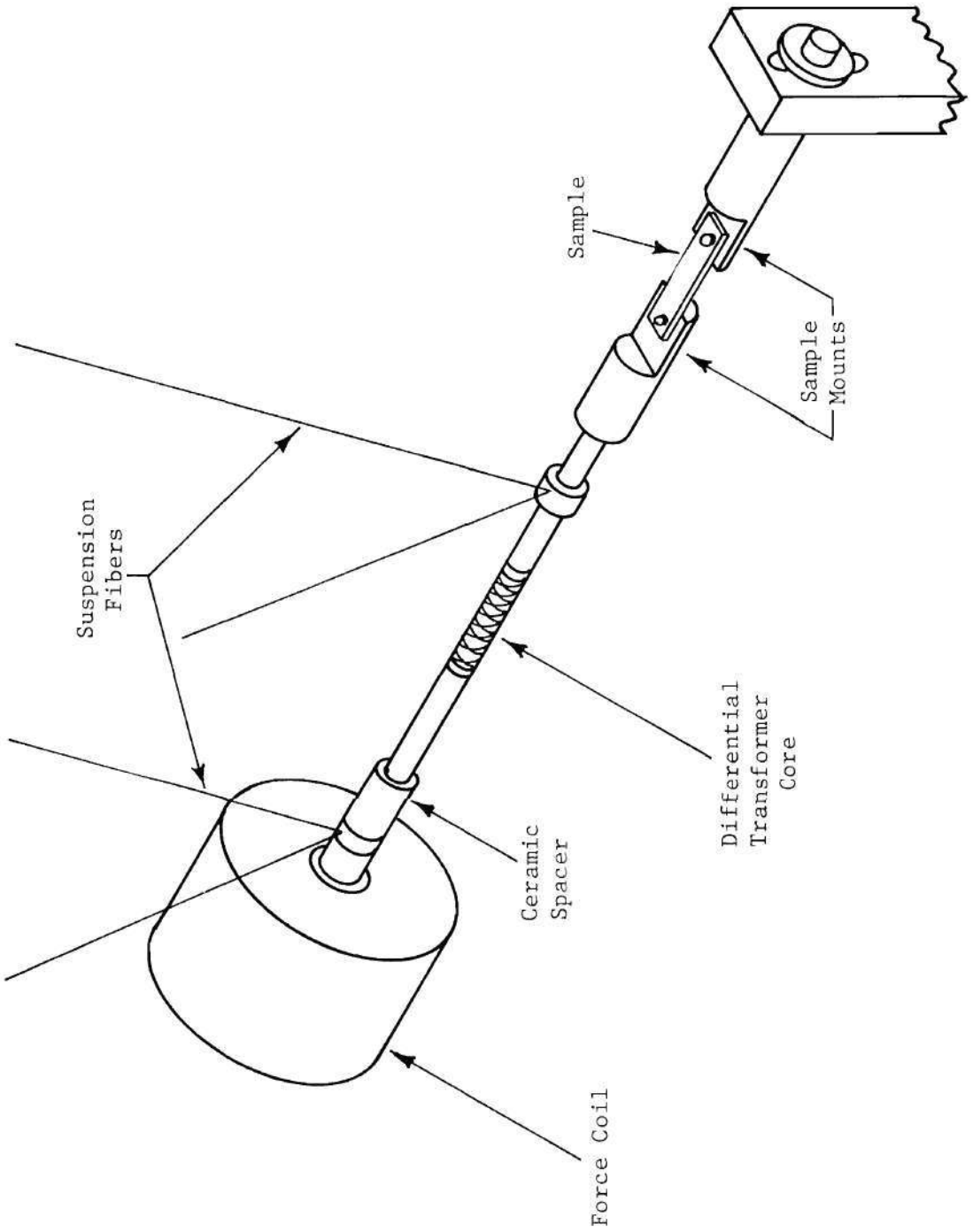

Figure 21. Schematic of Force Arm Assembly.

and 2.0 inch in diameter. The outer pole piece of the magnet has a thickness of 0.5 inch so that the number of turns in the magnetic field remains constant over a displacement range much greater than is usually required. The coil form was split and reinforced with epoxy to reduce eddy current dampening and thereby to increase the system response. Sufficient dampening remains to minimize vibration noise. The two segments of the force arm on either side of the differential transformer core are 3/16 inch diameter 304 stainless steel rods threaded at each end. The ceramic spacer provides thermal isolation of the core since the force coil becomes warm at high loads.

Mechanical features of the apparatus are shown in Figure 22. The magnet, transducer coil, mounting clamps and end post are mounted on sliding blocks which clamp to a 1 x 2 inch cross section stainless steel force bar having precision ground ways. A superstructure for the suspension fibers rides on parallel bars located on either side of the force bar. Except where dictated by performance requirements, all mechanical members were constructed of 304 stainless steel and surface ground to minimize stray magnetic field and ultra high vacuum problems.

The magnet is the type used to drive a large University loud speaker with an enlarged gap. The design of the magnet support block allows small alignment adjustments in all degrees of freedom. The differential transformer coil is positioned about the free core on a microscope slide mechanism which permits transducer zero adjustments prior to a data run. The construction of the end post allows three dimensional alignment of the fixed mount.

Two clamps are available for supporting the sample mounts during

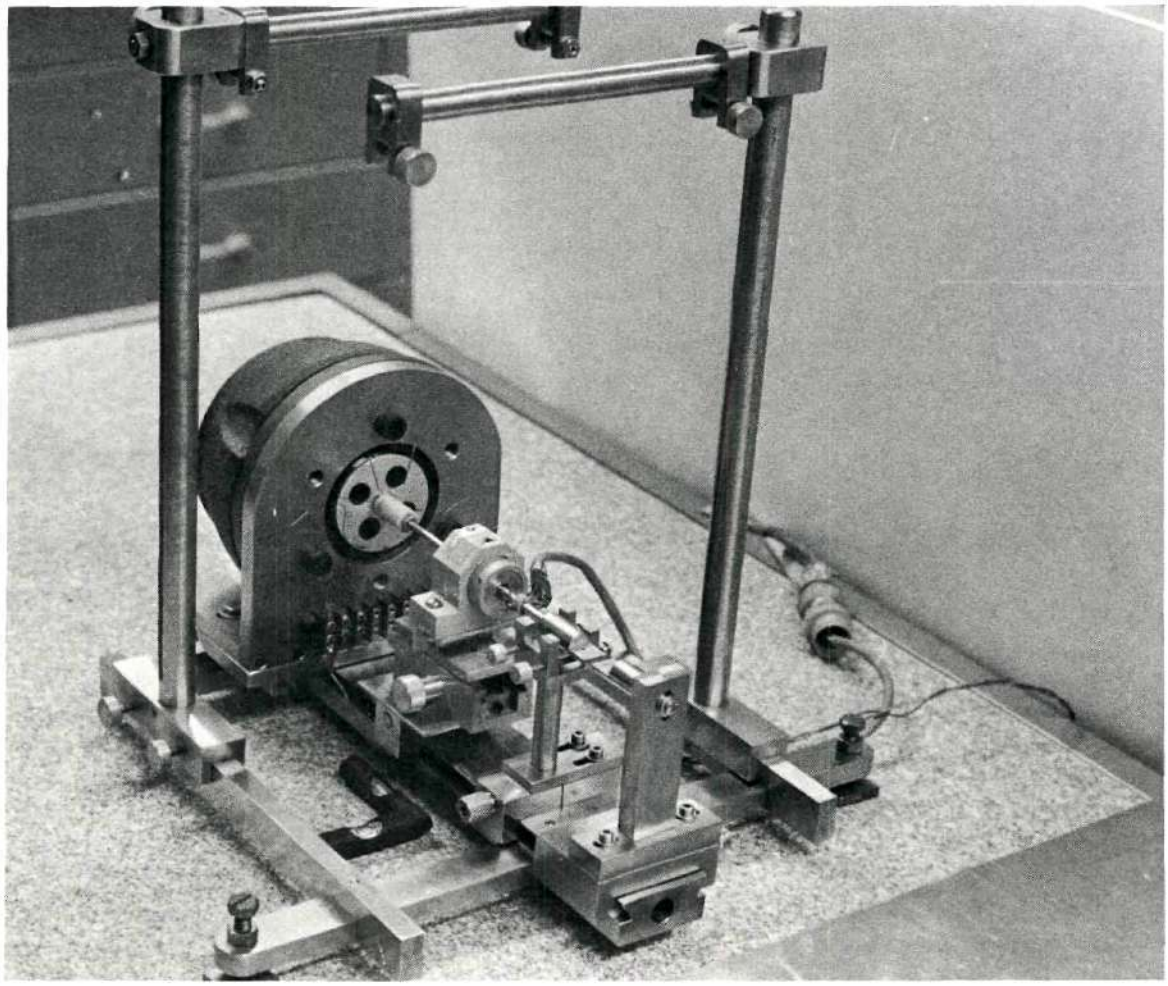

Figure 22. Mechanical Features of Microtensile Apparatus.

installation and removal of a test specimen. The particular mounts shown in Figure 22 require clamping of only the mount attached to the suspended force arm assembly but both ends must be clamped when the swivel mounts shown in Figure 23 are used. Only one of the two clamp assemblies is shown in Figure 23. Sufficient adjustment freedom is provided in the clamp assemblies so that the operations of clamping and release cause no motion of the mounts. Such motion could deform a single crystal specimen.

Elements of the fiber suspension superstructure provide a wide range of adjustment for achieving maximum stability. Precision positioning of the force arm assembly with the aligned components on the force bar is accomplished by fiber length admustments using a lock arrangement. Three leveling screws support the mechanical structure. Background vibrations are minimized by locating the apparatus on an air suspension table at atmospheric pressure. The entire vacuum system is positioned on a large air suspension slab when operated at ultra high vacuum.

Electronic Circuits

The electronic circuits provide for programmed stress application, monitoring the force signal and measurement of the sample strain. A linear stress rate is provided by driving a ten turn potentiometer with a synchronous motor. The resistance of the potentiometer controls a programmable power supply operated in the voltage regulated mode. The output of the power supply is applied to the force coil through a resistance panel. A range selector switch places a particular power

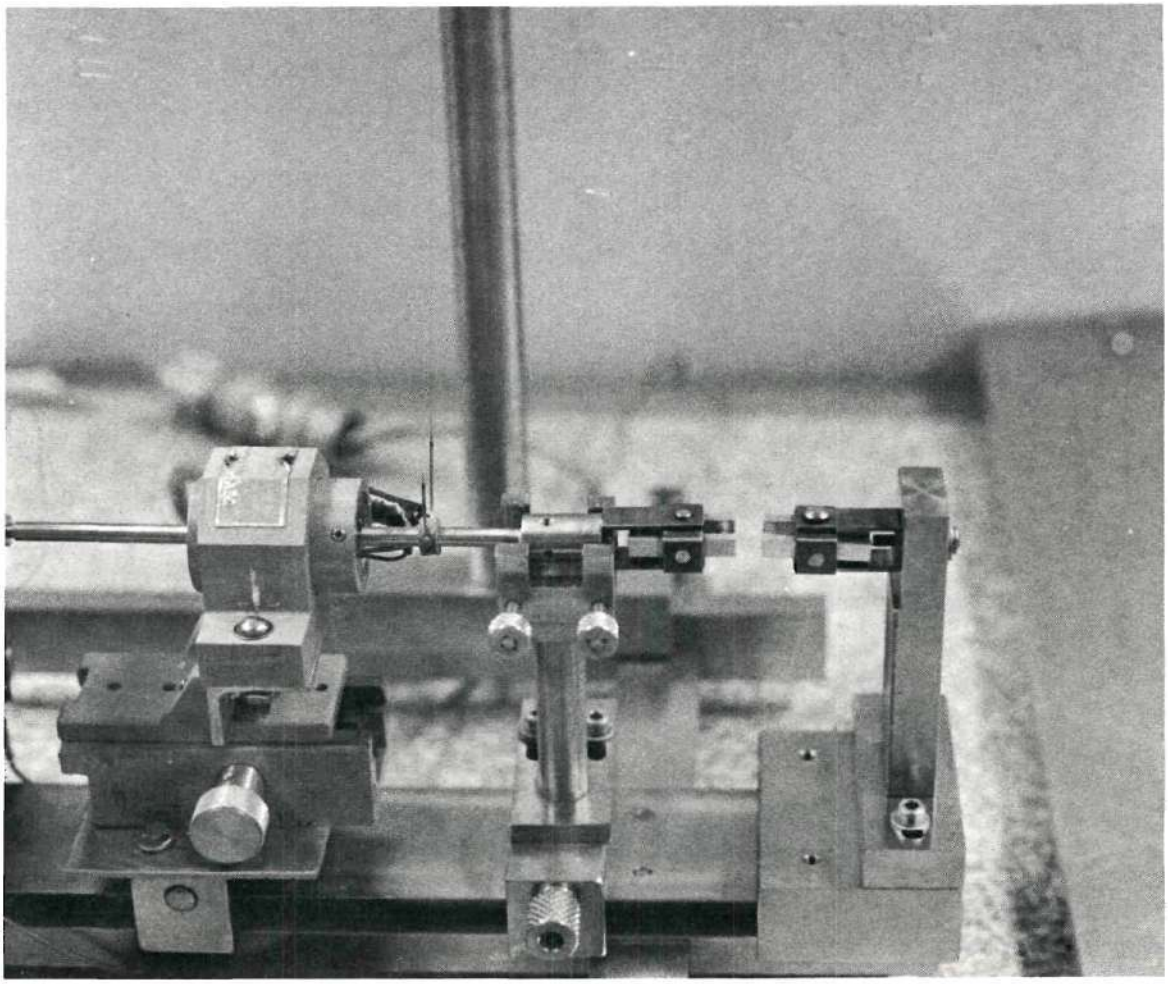

Figure 23. Microtensile Apparatus with Swivel Mounts Installed.

rheostat and precision metering resistor in series with the force coil according to the desired force range. Since the power supply is operated in voltage mode, a desired stress application rate may be selected by adjustment of the rheostat. Force coil current is monitored by feeding the potential drop across the metering resistor to the y-axis input of an x-y recorder. A signal proportional to the sample strain obtained from the differential transformer circuits is applied to the x-axis input of the recorder.

Operation

Calibration

The force applied to a sample through the force arm assembly is directly proportional to the coil current. Calibration of a force coil at higher loads is accomplished by hanging standard weights from a thread attached to the sample mount after passing over a pully. Calibration is checked at low forces using a transducer. Displacement calibrations are made using a ball tipped micrometer head fixed in one of the sample mounting clamps. A small reversed coil current insures contact between the end of the sample mount and the micrometer. Although the output of the transducer was found to be slightly nonlinear, displacement readings were reproducable to better than 0.5%. A calibration scale reflecting the transducer characteristics was prepared and used to correct for nonlinearity at the time resolved shear strains were computed.

Sample Mounting

Thin copper single crystal samples to be tested in tension are attached to metal tabs. The tabs are first aligned over a grid with

the proper spacing for the particular sample to be tested. An "L" shaped paper card is glued to side extensions of the tabs to maintain alignment and to protect the sample during subsequent mounting procedures. Samples are attached to the tabs using an adhesive or by soldering if the required heating does not adversely affect the sample. Eastman 910 adhesive was found convenient for copper crystals. Cementing a 0.020 inch high strength titanium alloy section on tabs in place of a normal sample showed that yielding of the bonds and other parts of the machine is negligible for the force ranges of interest in the thin single crystal studies. Although the Eastmen 910 adhesive bonds were usually strong enough after about 10 minutes, bond failures were eliminated by waiting at least 24 hours before testing.

Prior to mounting a specimen, alignment adjustments are made as described above. Holes in the tabs are slightly oversized so that final alignment of the specimen axis with the force arm axis can be made as the tabs are bolted in place. After the card is clipped the mounting clamps are relaxed with great care leaving the sample free for testing as shown in Figure 24. After the deformation is completed a second "L" shaped card is carefully glued across the clipped gap and the sample is removed without further deformation by reversing the procedure outlined above.

The swivel mounts shown in Figure 23 simplify alignment procedures as they allow rotation about vertical and horizontal axes and horizontal displacement perpendicular to the stress axis. The center of mass of the swivel members is located at the intersection of the two pivot axes to insure that no sample loading occurs due to the weight of sample

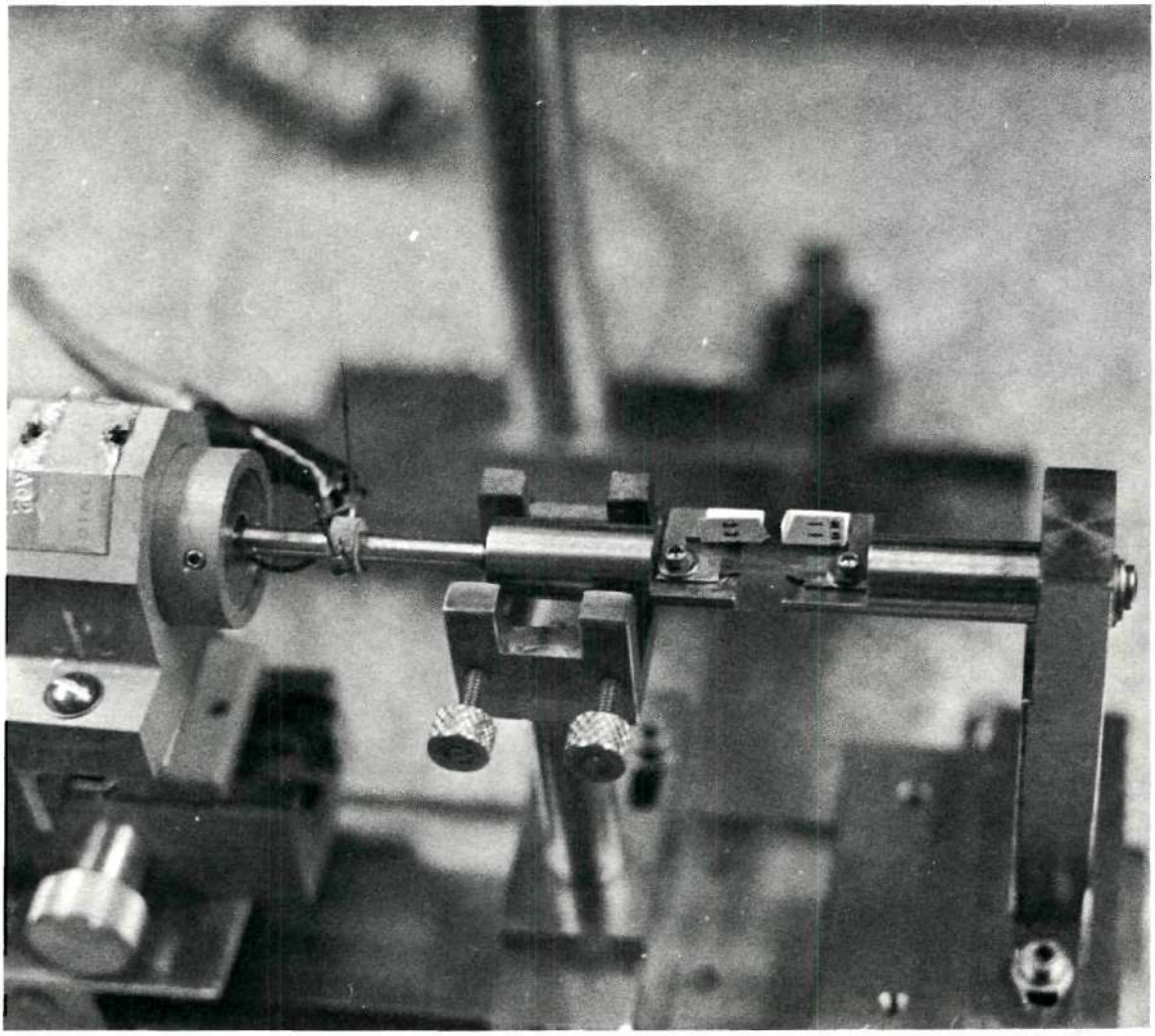

Figure 24. Specimen Mounted for Testing.

mounts. However, while stressing a specimen the swivel mounts displace a few ten thousandths of an inch taking up slack in the pivot pens. For most investigations this is not a serious problem and the self-aligning feature is a valuable asset.

Other mounting schemes allow testing in a bending mode. In addition, the use of inverted U-shaped mounting brackets permit tests with a sample immersed in a temperature bath, a corrosive medium or in an electrolytic solution with the sample serving as one electrode.

Performance

The force range is from a few dynes to about 120 newtons where several different coil and force arm configurations are employed. Vibrations, convection currents, the displaced pendulum and differential transformer interactions present the primary problems with low forces. Joule heating in the coil limits the maximum continuous force. Several free core differential transformers having maximum linear ranges between 0.3 inch and .003 inch provide flexibility in displacement measurements. An optical extensiometer can be devised if the differential transformer is not suited to a specific application.

Vibration problems are minimized by a combination of factors including the choice of laboratory site, an air suspension table, instrument structural design and experimental technique. The response of the system is determined by details of the force arm assembly. Although the response is low, a relatively massive force arm with eddy current dampening in the coil form is found best suited for low stress rates at force levels of a gram or more. The mass and dampening provides greater stability and larger force arm members minimize displacement of the

in the machine. A much faster response, equivalent to a few tens of Hertz, has been obtained using a speaker voice coil to drive a force arm constructed of thin wall aluminum tubing.

Applications

The microtensile apparatus has been used to study interface effects on the mechanical behavior of thin single crystals. It has also been used for routine measurements of the elastic modulus and fracture strength of graphite fibers and polycrystalline foils. The configuration of the machine is convenient for motion pictures of specimens to be made during deformation for correlations between emerging slip traces and stress strain curves. The mechanical behavior of the surface regions subjected to various corrosive liquids may also be investigated. A prototype version of the apparatus described here was used to investigate the mechanical behavior of thin foils of titanium alloys with the stressed sample an electrode in an electrolyte cell.

The operational principle of the system also permits fatigue deformation either by driving the programmable power supply with a desired wave form or by driving the force coil directly using an audio amplifier and oscillator. Relatively complex stress-time patterns are conveniently applied limited only by the inertia and dampening of the force arm assembly.

The apparatus has proved to be a reliable and versatile instrument for a wide variety of applications. Although certain features are necessarily delicate, operational procedures are simple and straight forward. Broken suspension fibers occur but can be replaced and the system realigned in a few minutes.

APPENDIX C

INTERFACE MODELS

The mechanical effects of two interface factors were evaluated using the simple theoretical treatments outlined in this section. In the first part the dislocation image concept of Eshelby[4] was employed to calculate the magnitude of strengthening expected for an abrupt, positive modulus discontinuity. The thin coating model of Head[5] was adapted to the specific interface materials and geometry used in these investigations. The second part outlines a calculation of strengthening effects expected from interfacial and surface energy considerations for the interfaces used here.

Image Stress Contributions

Dislocation Stress Components

The elastic stress field resulting from the presence of a dislocation accounts for most important dislocation interactions with other dislocations and with such features as grain boundaries, precipitates and surfaces. If the medium about a dislocation is isotropic then the resulting stress field can be expressed in terms of the components of a stress tensor. For a screw dislocation lying along the z axis the stress tensor components in cylindrical coordinates are[3]

$$\sigma_{\theta z} = \frac{\mu b}{2\pi r}$$

$$\sigma_{rz} = \sigma_{r\theta} = \sigma_{rr} = \sigma_{\theta\theta} = \sigma_{zz} = 0 \qquad (1)$$

where μ is the shear modulus of elasticity, b is the magnitude of the Burgers vector and r is the radius of the cylinder about the dislocation line on which the stress component would be measured.

From an edge type dislocation[3]

$$\sigma_{rr} = \sigma_{\theta\theta} = -\frac{\mu b \sin\theta}{2\pi(1-\nu)r}$$

$$\sigma_{r\theta} = \frac{\mu b \cos\theta}{2\pi(1-\nu)r} \qquad (2)$$

$$\sigma_{zz} = \nu(\sigma_{rr} + \sigma_{\theta\theta})$$

and

$$\sigma_{rz} = \sigma_{\theta z} = 0$$

where ν is Poisson's ratio. It is significant that all the non-vanishing stress tensor components expressed in cylindrical coordinates vary as $1/r$.

The energy per unit length, W, associated with a dislocation is the sum of the energy in the elastic stress field, W_e, and the energy of the dislocation core, W_c, where the crystal is strained beyond the elastic limit.

$$W = W_e + W_c \ . \qquad (3)$$

The elastic energy, W_e, of a straight, general dislocation having both screw and edge components is given in the expression:[2]

$$W_e = \frac{\pi b^2}{4\pi K} \ln \frac{r_1}{r_0} \ ; \ r_1 > r_0 \qquad (4)$$

$$\text{where} \qquad K = \cos^2\beta + \frac{\sin^2\beta}{(1-\nu)}$$

Here r_1 is the radius of the cylinder enclosing the elastic medium affected by the stress field of the dislocation and r_0 is the radius of a cylinder enclosing only the core. The dislocation line makes an angle β with its Burgers vector. An explicit expression for W_c is not required for the following discussions. It is sufficient to note that r_0 is usually considered to be less than 2b.

Although a dislocation is a defect and not a physical body it is found useful to describe interactions between a dislocation and a stress field resulting from an applied load, another dislocation or to the effect of a medium discontinuity in terms of "forces" and "torques" on the dislocation in question. Force magnitudes between dislocations vary with the inverse of their separation distance. Since the stress field of a dislocation varies as 1/r and the energy per unit length varies as the logarithm of r it is clear that the interactions of an isolated dislocation in a crystal are long range interactions.

Image Stress Calculations

The interaction force on a single screw dislocation due to an elastic modulus difference across an abrupt interface is considered. The dislocation is assumed parallel to a planar interface with slip plane and direction normal to the interface. Following Head,[5] the interaction force may be computed by postulating an infinite set of image dislocations. The real dislocation having Burgers vector b is located at x = a, y = 0 in a semi-infinite, isotropic medium of shear modules μ_1 as shown in Figure 25. The coating has thickness, t, and shear modulus, μ_2. The image dislocations are therefore located at the positions x_i, y = 0 and have Burgers vectors, b_i.

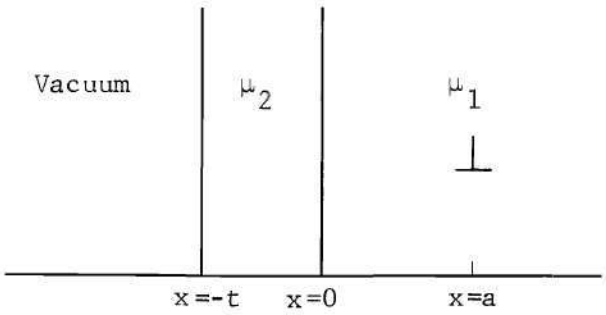

Figure 25. Schematic of Dislocation Near Interface of Surface Coating

$$x_1 = -a,\ x_2 = -(a + 2t),\ x_3 = -(a + 4t),\ ---,$$

$$x_n = -[a + 2(n - 1)t] \text{ for } n \geq 2$$

$$b_1 = \kappa b,\ b_2 = -(1 - \kappa^2)b,\ b_3 = -(1 - \kappa^2)\kappa b,\ ---, \tag{5}$$

$$b_n = -(1 - \kappa^2)\kappa^{n-2}b \text{ for } n \geq 2$$

where $\kappa = (\mu_2 - \mu_1)/(\mu_2 + \mu_1)$.

The force per unit length between two parallel screw dislocations having Burgers vectors b' and b'', separated by a distance r has only a radial component given by[2]

$$F = \frac{\mu b'b''}{2\pi r} . \tag{6}$$

The images therefore result in an infinite series of force terms, F_i, acting on the real dislocation. The individual terms derived from equations 5 and 6 are

$$F_1 = \frac{\mu_1 b^2 \kappa}{4\pi a}$$

$$F_2 = -\frac{\mu_1 b^2 (1 - \kappa^2)}{4\pi (a + t)} \tag{7}$$

$$F_3 = -\frac{\mu_1 b^2 (1 - \kappa^2)\kappa}{4\pi (a + 2t)} \text{ , etc.}$$

where positive and negative signs denote repulsion and attraction, respectively, by the interface. The resultant force on the dislocation is found from

$$F = \sum_{n=1}^{\infty} F_i \ . \tag{8}$$

Substituting the indicated terms of equation 7 into equation 8 the resultant force may be expressed in the form

$$F = \frac{\mu_1 b^2}{4\pi a} \left[\kappa - (1 - \kappa^2) \sum_{n=1}^{\infty} \frac{\kappa^{n-1}}{1 + nr} \right] \tag{9}$$

where $r = t/a$. It is convenient to represent the dimensionless quantity in the bracket by the symbol Q so that equation 9 becomes

$$F = \frac{\mu_1 b^2}{4\pi a} Q \ . \tag{10}$$

From the fundamental definition of an external force on a dislocation, the effective shear stress for the simple configuration assumed here is given by

$$\tau = \frac{F}{b} \ . \tag{11}$$

The applied resolved shear stress required to overcome the effect of a modulus difference at an abrupt interface therefore has the magnitude but opposite sign of that determined from equation 11. Results of image force calculations may then be compared to measured stress values following an evaluation of the specific geometrical factors.

A Burroughs 5500 computer program was used to calculate Q and Q/a for the first forty terms contained in the summation of equation 9. Calculations for Cu-Ni and Cu-Co interfaces were carried out assuming the dislocation located in a semi-infinite copper crystal near an interface resulting from coatings having thicknesses ranging from 10 Å to 12,000 Å. For each coating thickness, Q was computed for dislocation positions, a, also ranging from 10 Å to 12,000 Å. Results of these calculations pertaining to the experimental investigations reported here are summarized in Figures 26-29.

For a copper crystal substrate, values of F and τ are evaluated from computed Q/a values using

$$F = 2.5 \times 10^3 \ [Q/a] \text{ dyne/cm}$$
$$\tau = 9.6 \times 10^9 \ [Q/a] \text{ dyne/cm}^2 \qquad (12)$$

where a is in angstrom units. The family of curves, Q versus t for specific values of a, plotted in Figures 26 and 27 provides a concise representation of the spatial regions where a dislocation is repelled or attracted by the interface as a function of coating thickness. For example, Figure 26 shows that dislocations closer than 500 Å to a Cu-Ni interface are repelled if the nickel thickness is greater than 2000 Å,

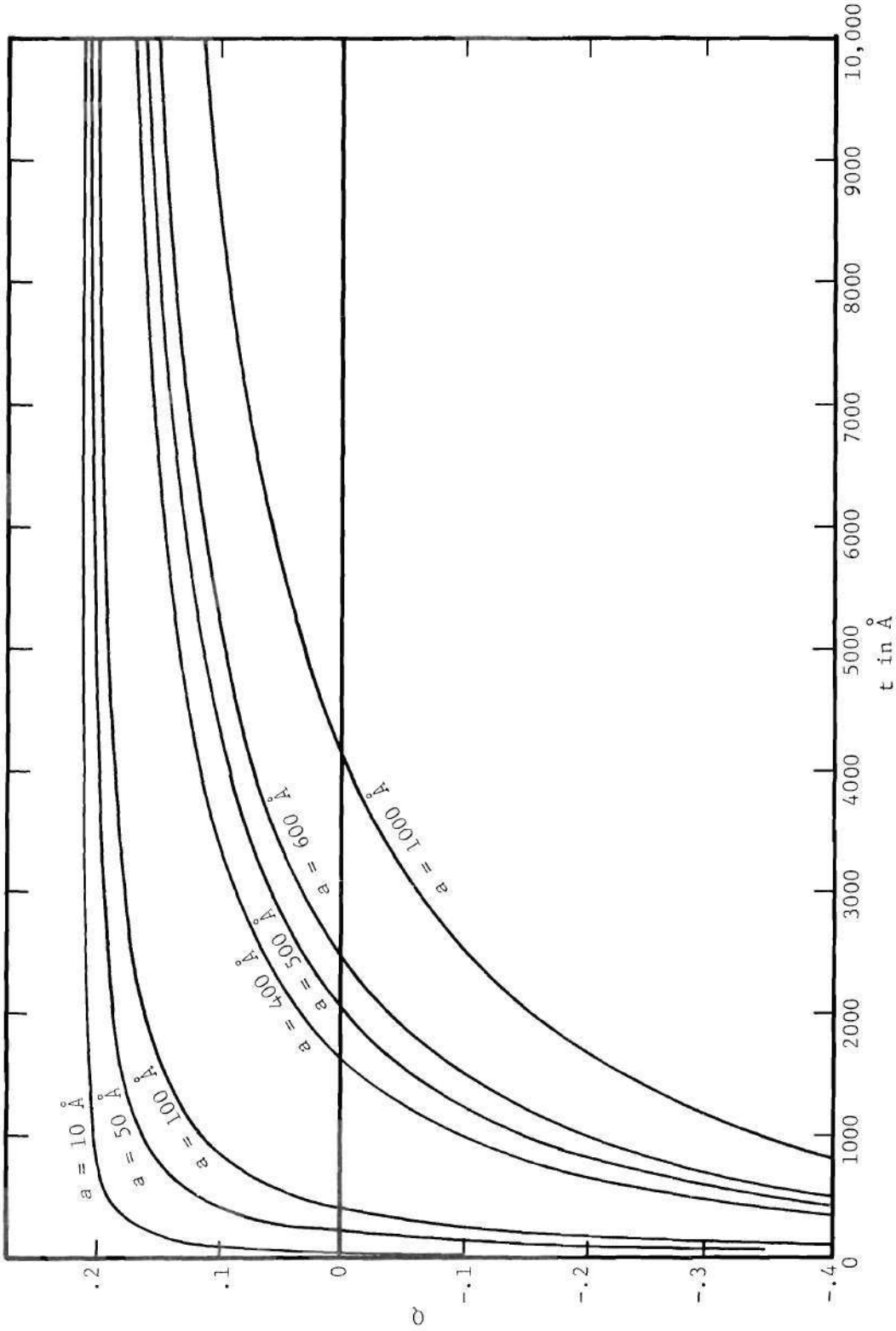

Figure 26. Plots of Calculated Values of Q Versus Coating Thickness, t, for Screw Dislocation Located Distance, a, from Cu - Ni Interface.

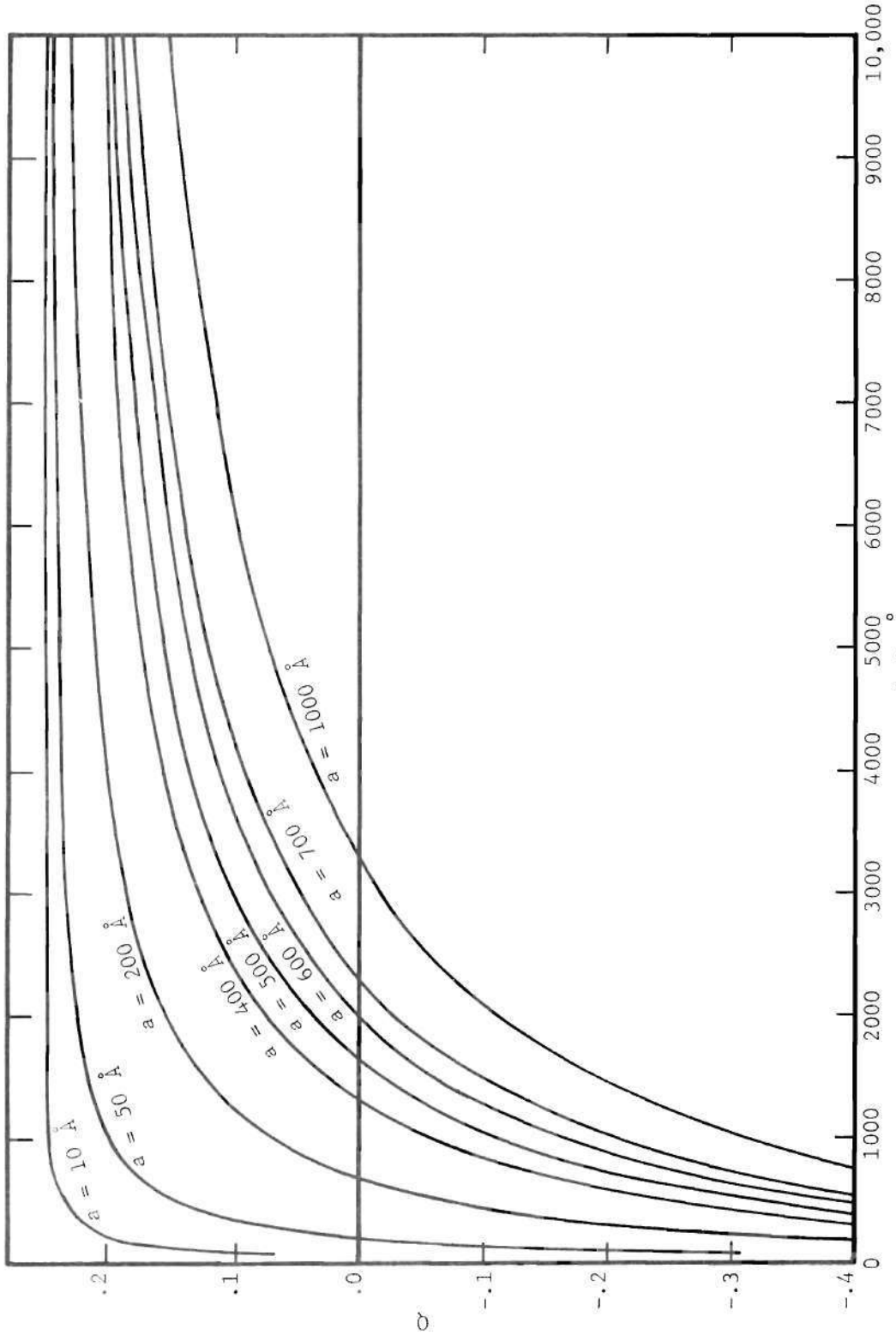

Figure 27. Plots of Q Versus Coating Thickness, t, for Screw Dislocation Located at Indicated Distances, a, from Cu - Co Interface.

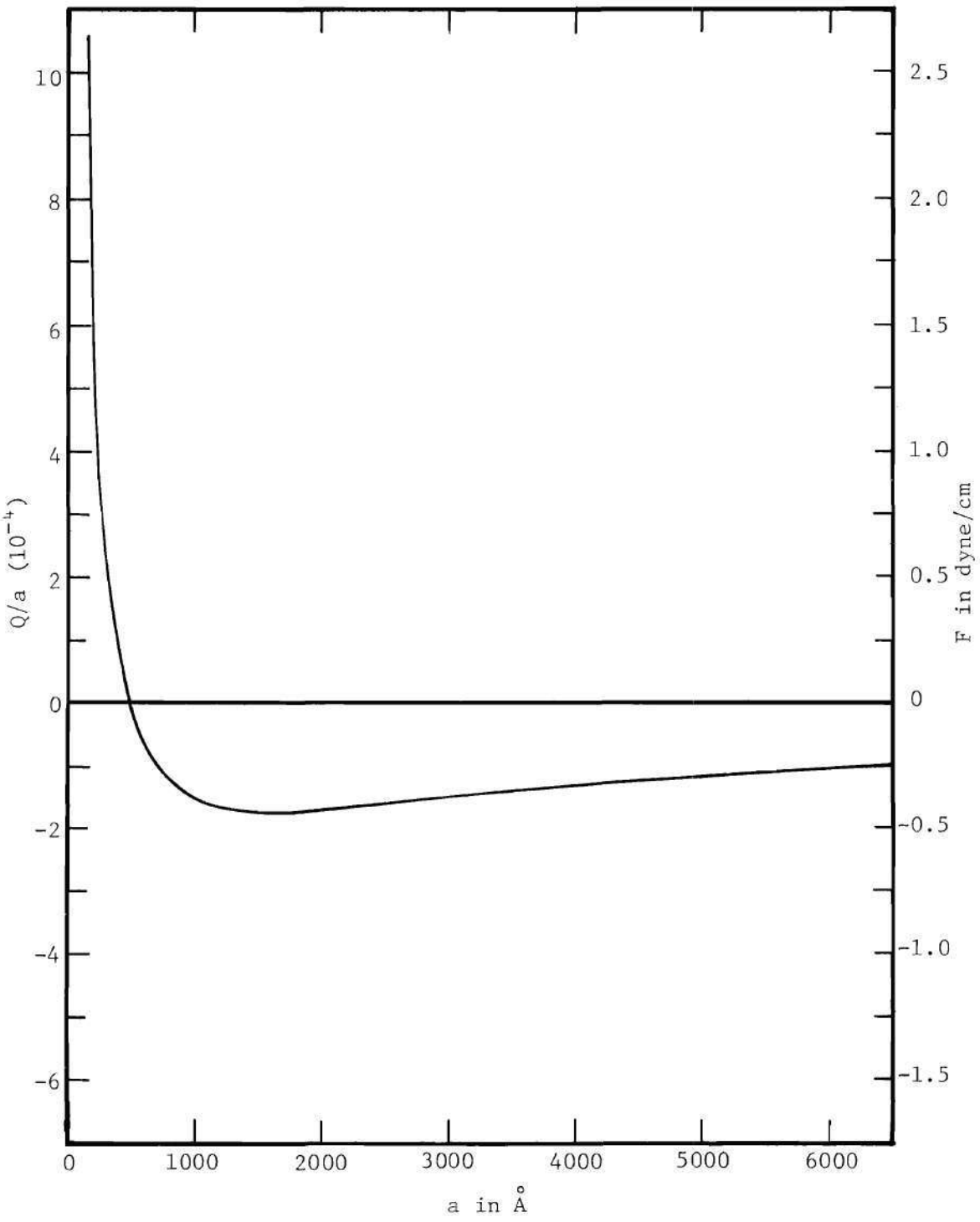

Figure 28. Plot of Q/a for 2000 Å Nickel Coating.

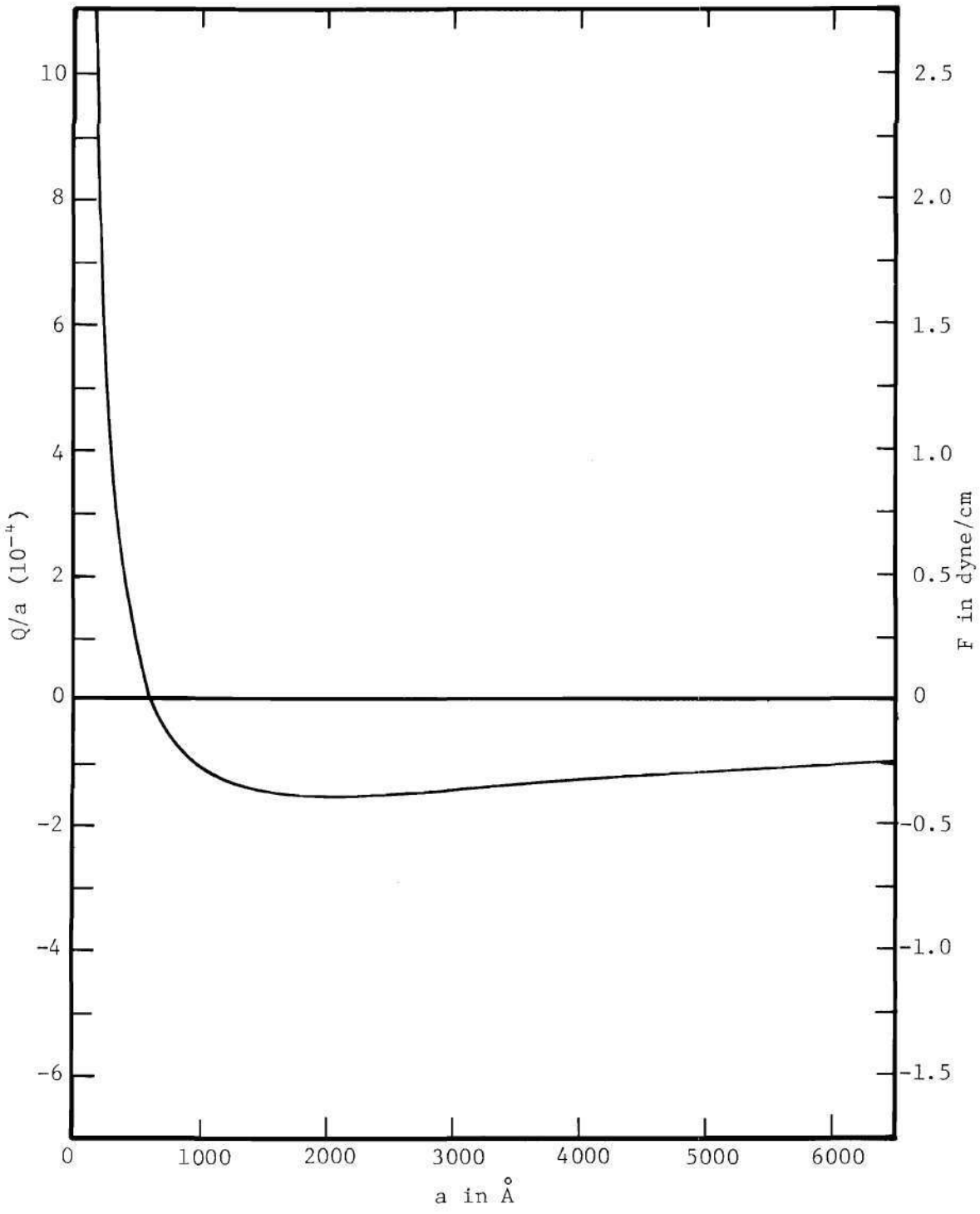

Figure 29. Plot of Q/a for 2000 Å Cobalt Coating.

which is approximately the coating thickness selected for these investigations. Similarly, Figure 27 indicates that for a = 500 Å, the dislocation is repelled for cobalt films thicker than 1700 Å.

For 2000 Å coating thicknesses the force is plotted as a function of dislocation position for Cu-Ni and Cu-Co interfaces respectively in Figures 28 and 29. Dislocation equilibrium positions are seen to occur at 500 Å for Cu-Ni and 600 Å for Cu-Co. For both interfaces, the magnitude of the repulsive force for dislocations closer than the equilibrium point are seen to be much greater than that of the attractive force beyond equilibrium. Force and shear stress values for a few dislocation positions in the neighborhood of 2000 Å coatings of nickel and cobalt are provided in Table 2.

TABLE 2

Representative Shear Stress and Dislocation Force Values Computed for 2000 Å Coatings

a Å	F_{Cu-Ni} $\frac{dyne}{cm}$	F_{Cu-Co} $\frac{dyne}{cm}$	τ_{Cu-Ni} $\frac{dyne}{cm^2}$	τ_{Cu-Co} $\frac{dyne}{cm^2}$
10	51	62	2.0×10^9	2.4×10^9
50	9.2	11.3	3.6×10^8	4.4×10^8
100	4.0	5.1	1.6×10^8	2.0×10^8
200	1.4	1.9	5.5×10^7	7.5×10^7
400	.20	.45	7.8×10^6	1.8×10^7
500	- .02	.18	$- 9 \times 10^5$	7.1×10^6
700	- .25	- .10	$- 1 \times 10^7$	$- 4.1 \times 10^6$
2,000	- .42	- .38	$- 1.7 \times 10^7$	$- 1.5 \times 10^7$
12,000	- .16	- .16	$- 6.4 \times 10^6$	$- 6.3 \times 10^6$

While an isotropic substrate medium is assumed throughout the above treatment, copper crystals are known to have anisotropic elastic constants. However, it is noted by Friedel[2] that the magnitude of necessary corrections to the dislocation stress energy when crystal anisotropy is taken into account is small. The additional computational complexity of a model which includes anisotropy is therefore not justified for purposes of comparison with results from a not too well defined actual interface.

The assumption of a perfect screw dislocation oriented parallel to the interface on a glide plane normal to the interface must also be examined with some care. Calculations for a dislocation having both screw and edge components would require a combination of the methods employed by both Head[5] and Conners.[9] However, the treatment of Conners for pure edge dislocations involved approximations which limited film thicknesses to values much less than those employed here.

The assumption that a dislocation line is parallel to the interface is not severe in that the spatial variation of the modulus interaction forces themselves will tend to produce this condition. The approximation is correct for a screw dislocation approaching a (111) major surface where the $\frac{a}{2}$ [110] Burgers vector lies parallel to the plane. The interaction force on a glide plane tilted by some angle, α, from the normal will have a component $F\cos\alpha$ acting on the dislocation. Depending upon the crystallographic orientation of the specimen, the interaction force should be somewhere between 0.5 and 1.0 of the value for an assumed normal plane.

Additional complexity is introduced by perfect dislocations separating into partials in materials where the stacking fault energy is low. Koehler's[12] calculation for the nickel-copper multiple layered structure showed that the low stacking fault energy reduces the repulsion from that expected for a perfect dislocation in copper by a factor of two.

Results of the above calculations provided a valuable intuitive guide for evaluating the magnitude and functional behavior expected for the modulus effect in spite of the obvious limitations of the model as discussed above. Figure 26 provided information for the selection of an optimum coating thickness for these investigations. A more elaborate model capable of treating variable Burgers vector directions would be particularly valuable for efforts in evaluating the magnitude of the modulus effect for specimen surfaces having various crystallographic orientations.

Surface and Interfacial Energy Contributions

For an uncoated tensile specimen of width w and thickness t, the load sharing by the surface tension prior to yielding is

$$F_f = \gamma_{10}(2w + 2t) \ . \tag{13}$$

The symbol γ_{10} represents the interfacial energy of an interface between the substrate material, 1, and a vacuum, 0. γ_{10} would be surface tension of the substrate material. For a thin specimen, where $t << w$, equation 13 becomes

$$F_f = 2w\gamma_{10} \ . \tag{14}$$

For a substrate coated with material, 2, of thickness a, we have in the elastic region

$$F_c = 2w(\gamma_{20} + \gamma_{12}) \tag{15}$$

where γ_{12} is the energy of the interface between the substrate and coating materials and γ_{20} is the surface tension of the coating material.

With the initiation of plastic deformation, discontinuities in the surface energy terms must be considered. Suppose the active slip plane makes an angle α between the surface trace of the slip plane and the stress axis as shown in Figure 30.

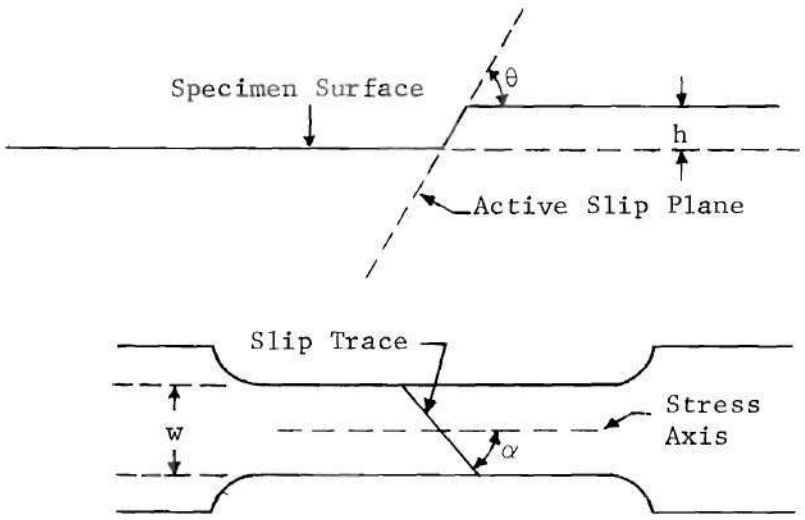

Figure 30. Schematic of Slip Trace at Surface of Specimen

It will be assumed that γ_{10} may, in this case, be treated as the increase in surface energy resulting from the creation, by slip, of unit area of new surface. The surface energy change, ΔE, for a slip step of height h is therefore given by

$$\Delta E = \frac{2wh\gamma_{10}}{\text{Sin } \theta \text{ Sin } \alpha} \tag{16}$$

where edge contributions are ignored. The component along the stress axis of the surface force contribution necessary for generation of the new surface area of the slip step is therefore

$$F_s = \frac{2w\gamma_{10}}{\text{Sin } \alpha \text{ Cos } \theta} \, . \tag{17}$$

One surface of a composite specimen with a slip step of height less than the coating thickness, a, is sketched in Figure 31.

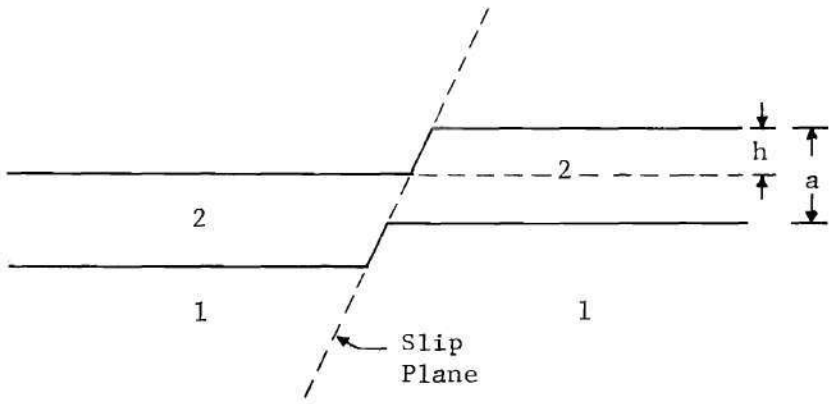

Figure 31. Schematic of Slip Step Through Coating

The force necessary to generate the configuration of Figure 31 is similarly written

$$F = \frac{2w}{\text{Sin } \alpha \text{ Cos } \theta} (\gamma_{12} + \gamma_{20}) \, . \tag{18}$$

The configuration for h > a is sketched in Figure 32.

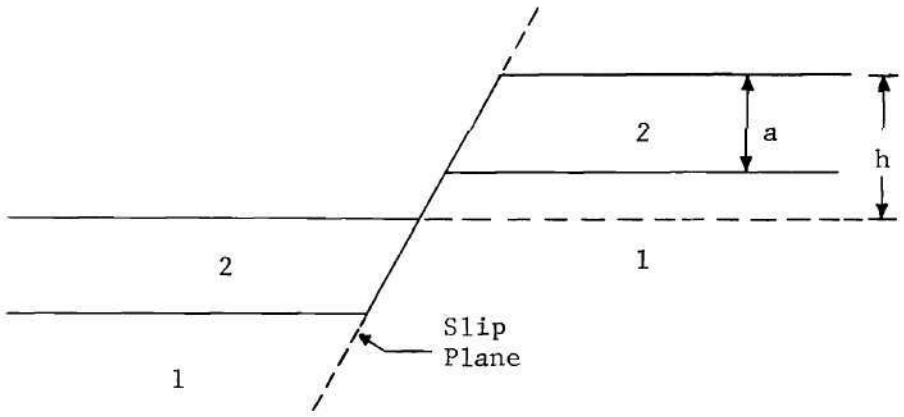

Figure 32. Schematic of Slip Step Having Height Greater Than Coating Thickness

The work required to generate this configuration is

$$\Delta E = \frac{2w}{\text{Sin } \theta \text{ Sin } \alpha} [\gamma_{20}a + \gamma_{10}(h - a) + \gamma_{12}a] \ . \qquad (19)$$

However, since a is constant, the surface force contribution for $h > a$ reduces to the expression of equation 17.

Treatment in further detail would involve considerations of the interfacial energy for specific crystallographic planes and the energetics of the planar discontinuities occuring at slip step corners. Measurements of the orientation dependence of the surface tension of copper[57] and nickel[58] have shown that the surface tension varies less than 3% between (100), (111) and (110) planes. The experimental uncertainty in available data for surface tensions and interfacial energies is much greater than the orientational variation. Apparently no data have been reported which would permit estimations of surface

or interfacial energies due to slip step corners. The corner energy should, however, depend upon the orientation of an active slip plane relative to the surface and the net contribution should be directly proportional to the fineness of slip.

The maximum load sharing calculated by substituting the usually listed interfacial and surface energy values in the above expressions represents less than 2% of the load at yield for specimens measured here. However, surface and interfacial energy contributions may become a significant fraction of the normal strength of a single crystal for specimen thicknesses less than a few microns. For example, a specimen 2 mm wide and 1 micron thick would yield with a load of about 1,000 dyne assuming a bulk yield stress of 5×10^7 dyne/cm^2. A surface tension of 1,750 dyne/cm would support a load of about 700 dyne for a specimen of these dimensions. Menter and Pashley[59] concluded the surface tension contribution was negligible for thin film thicknesses greater than 100 - 200 Å. However, the results they were quoting assumed very high film strengths and it is not clear how bulk and surface strengthening effects were separated. Surface or interfacial energy contributions to mechanical strengthening must be taken into account for specimen configurations or materials, such as binary alloys, where the ratio of interface area to volume is large.

BIBLIOGRAPHY

1. J. Weertman and J. R. Weertman, Elementary Dislocation Theory, Macmillan Co., New York, 1964.

2. J. Friedel, Dislocations, Pergamon Press, 1964.

3. J. P. Hirth and Jens Lothe, Theory of Dislocations, McGraw-Hill, New York, 1968.

4. J. D. Eshelby, Phil. Trans., A-244, 87 (1951).

5. A. K. Head, Phil. Mag., 44, 92 (1953).

6. A. K. Head, Austr. J. Phys., 13, 278 (1960).

7. J. D. Eshelby and A. N. Stroh, Phil. Mag., 42, 1401 (1951).

8. E. H. Yoffe, Phil. Mag., 6, 1147 (1961).

9. G. H. Conners, Int. J. Engng. Sci., 5, 25 (1967).

10. M. B. McNeil and J. C. Grosskreutz, J. Appl. Phys., 38, 3310 (1967).

11. J. F. Prins and H. G. F. Wilsdorf, Canad. J. Phys., 45, 1177 (1967).

12. J. S. Koehler, Phys. Rev., B2, 547 (1970).

13. R. L. Fleischer, Acta Met., 8, 598 (1960).

14. R. Roscoe, Phil. Mag., 21, 399 (1936).

15. C. S. Barrett, P. M. Aziz and I. Markson, Trans. AIME, 197, 1655 (1953).

16. J. J. Gilman and T. A. Read, Trans. AIME, 194, 875 (1952).

17. D. R. Brame and T. Evans, Phil. Mag., 3, 971 (1958).

18. T. Evans and D. R. Schwarzenberger, Phil. Mag., 4, 889 (1959).

19. J. C. Grosskreutz, Surf. Sci., 8, 173 (1967).

20. R. M. Latanision and R. W. Staehle, Acta. Met., 17, 307 (1969).

21. G. E. Ruddle and H. G. F. Wilsdorf, Appl. Phys. Letters, 12, 271 (1968).

22. R. M. Johnson and R. J. Block, Acta Met., 16, 831 (1968).

23. L. C. DeJonghe and I. G. Greenfield, Acta Met., 17, 1411 (1969).

24. W. R. Patterson and I. G. Greenfield, Acta Met., 19, 123 (1971).

25. J. V. Pridans and J. C. Bilello, AIME Spring Meeting, Atlanta, Ga., May 18, 1971; J. V. Pridans, MS Thesis, State University of New York at Stony Brook (1971).

26. J. H. van der Merwe in Single Crystal Films (edited by M. Francombe and H. Sato), p. 139, Pergamon Press, Oxford, 1964.

27. J. W. Matthews in Single Crystal Films, p. 165.

28. J. W. Matthews, Phil. Mag., 13, 1207 (1966).

29. J. W. Matthews and W. A. Jesser, Acta Met., 15, 595 (1967).

30. W. A. Jesser and J. W. Matthews, Phil. Mag., 17, 461 (1968).

31. A. I. Fedorenko and R. Vincent, Phil. Mag., 24, 55 (1971).

32. W. A. Jesser and D. Kuhlmann-Wilsdorf, Phys. Stat. Sol., 19, 95 (1967).

33. A. R. C. Westwood, D. L. Goldheim and R. G. Lye, Phil. Mag., 16, 505 (1967).

34. A. R. C. Westwood, D. L. Goldheim and R. G. Lye, Phil. Mag., 17, 951 (1968).

35. A. R. C. Westwood in Strengthening Mechanisms-Metals and Ceramics, p. 407, Syracuse Univ. Press, 1966.

36. I. R. Kramer, Trans. Met. Soc. AIME, 230, 991 (1964).

37. A. R. C. Westwood, Phil. Mag. 8th Ser., 5, 981 (1960).

38. J. H. Westbrook and J. J. Gilman, J. Appl. Phys., 33, 2360 (1962).

39. A. R. C. Westwood, D. L. Goldheim and E. N. Pugh, Phil. Mag., 15, 105 (1967).

40. A. R. C. Westwood, C. M. Preece and M. H. Damdar, "Adsorption-Induced Brittle Fracture in Liquid Metal Environments," May 1967, Martin-Marietta, RIAS Tech. Report No. 67-8c.

41. J. C. Grosskreutz and C. Q. Bowles in Environment-Sensitive Mechanical Behavior (edited by A. R. C. Westwood and N. S. Stoloff), Gordon and Breach Science Publishers, New York, 1966.

42. I. R. Kramer and L. J. Demer, "Effects of Environment on Mechanical Properties of Metals" in Progress in Materials Science, Vol. 9, Pergamon Press, 1961.

43. I. R. Kramer, Trans. Met. Soc. AIME, 221 (1961).

44. I. R. Kramer, Trans. Met. Soc. AIME, 227 (1963).

45. V. I. Likhtman, P. A. Rebinder and G. V. Karpenko, Effect of Surface-Active Media on the Deformation of Metals, Translated from the Russian in 1960, Chemical Publishing Co., Inc., New York.

46. D. H. Bradhurst and J. S. L. Leach, Trans. Brit. Ceram. Soc., 62, 793 (1963).

47. B. D. Cullity, Elements of X-Ray Diffraction, Addison-Wesley, Reading, Mass., 1956.

48. B. R. Livesay, L. K. Jordan and E. J. Scheibner, J. Appl. Phys., 37, 1266 (1966).

49. R. M. Bozarth, Ferromagnetism, D. van Nostrand, Inc., New York, 1951.

50. B. Rossi, Optics, Addison-Wesley, Reading, Mass., 1957.

51. D. Hull in Deformation Twinning, Gordon and Breach, New York, p. 121 (1964).

52. T. H. Blewitt, R. R. Coltman and J. K. Redman, Jour. Appl. Phys., 28, 651 (1957).

53. J. H. Venables in Deformation Twinning, Gordon and Breach, New York, p. 77 (1957).

54. K. Kuhlmann-Wilsdorf and K. Srinivasa Raghavan, Rev. Sci. Instr., 33, 930 (1962).

55. D. M. Marsh, J. Sci. Instrum., 38, 229 (1961).

56. S. S. Brenner, J. Appl. Phys., 28, 1023 (1957).

57. W. M. Robertson and P. B. Shewmon, Met. Trans. AIME, 224, 804 (1962).

58. H. Mykura, Acta. Met., 9, 570 (1961).

59. J. W. Menter and D. W. Pashley in Structure and Properties of Thin Films, p. 111, Wiley and Sons, Inc., 1959.

VITA

Billy R. Livesay was born the son of Mr. and Mrs. M. E. Livesay September 17, 1933 in Fort Worth, Texas. There he attended public schools and graduated from North Side High School in 1951. He received a Bachelor of Arts in Physics from Texas Christian University in 1955 and a Master of Arts in Physics from the University of Texas in 1957.

After a tour as a Second Lieutenant in the U. S. Army Signal Corps, he came to the Georgia Institute of Technology as a Physics Instructor in 1958. He subsequently joined the research staff of the Engineering Experiment Station in 1961 where he is currently a Research Scientist in the Physical Sciences Division.

He married Martha Ann Schroeder in 1952. They have three children, Constance Ruth, Catherine Ellen, and William Douglas.